

# The magnetopause deformation indicated by fast cold ion motion

Wenlong Guo<sup>1</sup>, Binbin Tang<sup>2</sup>, Qing-He Zhang<sup>1</sup>, Wenya Li<sup>3</sup>, Zhongwei Yang<sup>4</sup>, Tianran Sun<sup>3</sup>, Jiuqi Ma<sup>5</sup>, Xiaoxin Zhang<sup>6</sup>, Xiaocheng Guo<sup>3</sup>, and Chi Wang<sup>3</sup>

<sup>1</sup>Institute of Space Sciences, Shangdong University

<sup>2</sup>National Space Science Center, CAS

<sup>3</sup>National Space Science Center, Chinese Academy of Sciences

<sup>4</sup>State Key Laboratory of Space Weather, National space science center

<sup>5</sup>University of Science and Technology of China

<sup>6</sup>China Meteorological Administration

October 27, 2023

## Abstract

The magnetopause deformation due to the upstream magnetosheath pressure perturbations is important to understand the solar wind - magnetosphere coupling process, but how to identify such events from in-situ spacecraft observations is still challenging. In this study, we investigate magnetopause crossing events with fast-moving cold ions in the magnetosphere from Magnetospheric Multiscale (MMS) observations, and find when fast-moving cold ions are present at the magnetopause, they are closely associated with the magnetopause deformation, which is featured by fast magnetopause motion and significant magnetopause normal deflection from model predictions. Therefore, fast-moving cold ions can be a useful indicator to search for magnetopause deformation events. By integrating the cold ion speed, the inferred magnetopause deformation amplitude varies from 0.2 to 2.5 RE. Further statistics indicate that such magnetopause deformation events prefer to occur under quasi-radial interplanetary magnetic field and fast solar wind conditions, suggesting high-speed magnetosheath jets could be one direct cause of magnetopause deformations.

# The magnetopause deformation indicated by fast cold ion motion

Wenlong Guo<sup>1</sup>, Binbin Tang<sup>2</sup>, Qinghe Zhang<sup>1</sup>, Wenya Li<sup>2</sup>, Zhongwei Yang<sup>2</sup>,  
Tianran Sun<sup>2</sup>, Jiuqi Ma<sup>3</sup>, Xiaoxin Zhang<sup>4</sup>, Xiaocheng Guo<sup>2</sup>, and Chi Wang<sup>2</sup>

<sup>1</sup>Shandong Provincial Key Laboratory of Optical Astronomy and Solar-Terrestrial Environment, Institute of Space Sciences, Shandong University, Weihai, China.

<sup>2</sup>State Key Laboratory of Space Weather, National Space Science Center, Chinese Academy of Sciences, Beijing, China.

<sup>3</sup>School of Earth and Space Sciences, University of Science and Technology of China, Hefei, China.

<sup>4</sup>Key Laboratory of Space Weather, National Center for SpaceWeather, China Meteorological Administration, Beijing, China.

## Key Points:

- The magnetopause is found to be significantly deformed with the presence of fast-moving cold ions, whose speed can exceed  $\sim 400 \text{ km s}^{-1}$ .
- The inferred magnetopause deformation amplitude varies from  $\sim 0.2$  to  $2.5 R_E$ .
- The observed magnetopause deformation prefers to occur under quasi-radial IMF and fast solar wind conditions.

---

Corresponding author: Binbin Tang and Qinghe Zhang, [bbtang@spaceweather.ac.cn](mailto:bbtang@spaceweather.ac.cn),  
[zhangqinghe@sdu.edu.cn](mailto:zhangqinghe@sdu.edu.cn)

## Abstract

The magnetopause deformation due to the upstream magnetosheath pressure perturbations is important to understand the solar wind - magnetosphere coupling process, but how to identify such events from in-situ spacecraft observations is still challenging. In this study, we investigate magnetopause crossing events with fast-moving cold ions in the magnetosphere from Magnetospheric Multiscale (MMS) observations, and find when fast-moving cold ions are present at the magnetopause, they are closely associated with the magnetopause deformation, which is featured by fast magnetopause motion and significant magnetopause normal deflection from model predictions. Therefore, fast-moving cold ions can be a useful indicator to search for magnetopause deformation events. By integrating the cold ion speed, the inferred magnetopause deformation amplitude varies from 0.2 to  $\sim 2.5 R_E$ . Further statistics indicate that such magnetopause deformation events prefer to occur under quasi-radial interplanetary magnetic field and fast solar wind conditions, suggesting high-speed magnetosheath jets could be one direct cause of magnetopause deformations.

## 1 Introduction

The magnetopause is a boundary that shields the Earth's magnetosphere from the shocked solar wind. Its size and configuration are acutely important when investigating interactions between the interplanetary and magnetospheric environments, as various processes, such as magnetic reconnection and surface waves, can occur at the magnetopause, enabling mass and energy transfer across it.

To a first-order approximation, the magnetopause can be effectively represented through empirical models on large scales. For example, its shape and location have been extensively functioned (e.g. Fairfield, 1971; Shue et al., 1997, 1998; Lin et al., 2010; Dmitriev et al., 2011; Liu et al., 2015; Nguyen et al., 2022), which helps researchers to gain a preliminary understanding of the magnetopause by providing a basic response of the magnetopause under different solar wind and magnetospheric conditions. The accuracy of some widely used empirical magnetopause models has been tested with a large database of in-situ spacecraft crossings (Staples et al., 2020). The result shows that the magnetopause model can be used to estimate magnetopause location to within  $\pm 1$  Earth radii ( $R_E$ ) for the majority of magnetopause crossing events (74%), but sometimes discrepancies between measurements and model predictions can be large. This discrepancy can be partly attributed to the non-stationary nature of the magnetopause, which moves and changes under varying upstream plasma and magnetic field conditions. It is found that the usual magnetopause motion speed along its normal direction is around  $40 \text{ km s}^{-1}$  from in-situ spacecraft measurements (e.g. Phan & Paschmann, 1996; Paschmann et al., 2018), and the global simulations get a similar result (Xu et al., 2022). However, sometimes the magnetopause can move extremely fast, reaching to a speed over  $200 \text{ km s}^{-1}$  (Phan & Paschmann, 1996; Paschmann et al., 2018). Such fast magnetopause motion should be probably caused by rapid pressure variations in the upstream magnetosheath. Actually, the magnetosheath is highly turbulent (Karimabadi et al., 2014), and structures with transient pressure perturbations, such as mirror-mode waves, high-speed magnetosheath jets (HSJs), and downstream propagating solar wind/foreshock transients, can frequently occur. Impacts of these structures to the magnetopause can be hardly incorporated into empirical models due to their transient nature, but many related event studies have been performed.

Sibeck et al. (1999) has shown that the pressure within a hot flow anomaly (HFA, one typical solar wind transient structure) can be depressed by an order in magnitude with respect to the ambient background, allowing the magnetopause move outward about  $5 R_E$  in 7 minutes during the impacting process. Such HFA impact to the magnetopause has been displayed in different events, which in general can lead into the fast magnetopause

69 compression and expansion (Sibeck et al., 2000; Jacobsen et al., 2009; Šafránková et al.,  
70 2012; Zhang et al., 2022). Similarly, HSJs with local pressure enhancements can induce  
71 obvious inward magnetopause motion, following by possible subsequent magnetopause  
72 rebound (Shue et al., 2009; Plaschke et al., 2018; X. Wang et al., 2023) and the observed  
73 magnetopause normal can significantly differ from model predictions (Escoubet et al.,  
74 2020). Accompanied with the magnetopause deformation, magnetic reconnection can be  
75 triggered at the magnetopause (Hietala et al., 2018; Ng et al., 2021), waves can be gen-  
76 erated in the magnetosphere (Katsavrias et al., 2021), and the ionosphere can have some  
77 response as well (B. Wang et al., 2018). Therefore, investigations of the magnetopause  
78 deformation caused by these pressure perturbation structures are very helpful to under-  
79 stand the solar wind-magnetosphere coupling process, as their occurrence rates are not  
80 rare (Plaschke et al., 2016; Schwartz et al., 2000). However, due to limited cross-sections  
81 of these structures (for example, the spatial scale of HSJs varies from  $\sim 0.1$  to  $>1 R_E$  (Plaschke  
82 et al., 2016, 2020)), the investigation of their impact to the magnetopause is still insuf-  
83 ficient, which can be attributed to the difficulty in tracing the magnetopause response  
84 from in-situ spacecraft measurements.

85 Cold ions of ionospheric origin are often present in the magnetosphere (André &  
86 Cully, 2012). Due to the frozen-in nature of cold ions, they usually convect with mag-  
87 netic field lines in the direction perpendicular to the magnetic field and they can be de-  
88 tected by on board particle instruments when cold ions get a relatively large bulk en-  
89 ergy to overcome the spacecraft potential. Frequently, cold ions can reach to the mag-  
90 netopause, and evolve into processes at the magnetopause, such as magnetic reconnection  
91 (Toledo-Redondo et al., 2016, 2021; Li et al., 2017). The cold ion speed at the mag-  
92 netopause is often tens of  $\text{km s}^{-1}$ . In this study, we show that the speed of cold ions can  
93 reach to several hundreds of  $\text{km s}^{-1}$ , which can be taken as a good indicator for mag-  
94 netopause deformation, and the detection of fast-moving cold ions can be a useful tool  
95 to search for magnetopause deformation events.

## 96 2 Observation

97 In this study, we investigate magnetopause crossing events accompanied with fast-  
98 moving cold ions from MMS observations. We use magnetic field data from the fluxgate  
99 magnetometer (Russell et al., 2016), electric field data from the electric field double probes  
100 (Ergun et al., 2016; Lindqvist et al., 2016), and particle data from the fast plasma in-  
101 vestigation (Pollock et al., 2016). Due to the small separation of four MMS spacecraft  
102 (typically only a few to tens of kilometers at the magnetopause), data from individual  
103 satellites appear almost identical, and we primarily present the data from MMS 1. Un-  
104 less otherwise stated, all vectors are presented in geocentric solar magnetospheric (GSM)  
105 coordinates.

106 We select relevant magnetopause crossing events semi-manually using following cri-  
107 teria. First, the location where MMS cross the magnetopause is within a cone angle of  
108  $45^\circ$  centered on the Sun-Earth line, allowing us to focus on events near the subsolar re-  
109 gion. Second, the speed of cold ions is larger than  $200 \text{ km s}^{-1}$ , and  $V_x$  should be the ma-  
110 jor component. Third, sometimes cold ions are difficult to identify before reaching to the  
111 magnetopause, as they can be either heated or mixed with other ion populations in the  
112 magnetopause boundary layer. We limit the time difference between clear cold ion sig-  
113 natures and the magnetopause crossing is less than 10 seconds, ensuring that the cold  
114 ion motion can be closely related to the magnetopause. Finally, the interplanetary mag-  
115 netic field from OMNI should be stable at least for 15 min surrounding the magnetopause  
116 crossing, excluding the impact of the solar wind structures (such as magnetic disconti-  
117 nuities) to the magnetopause. If there are data gaps in the OMNI data set, we use time-  
118 shifted ACE data instead.

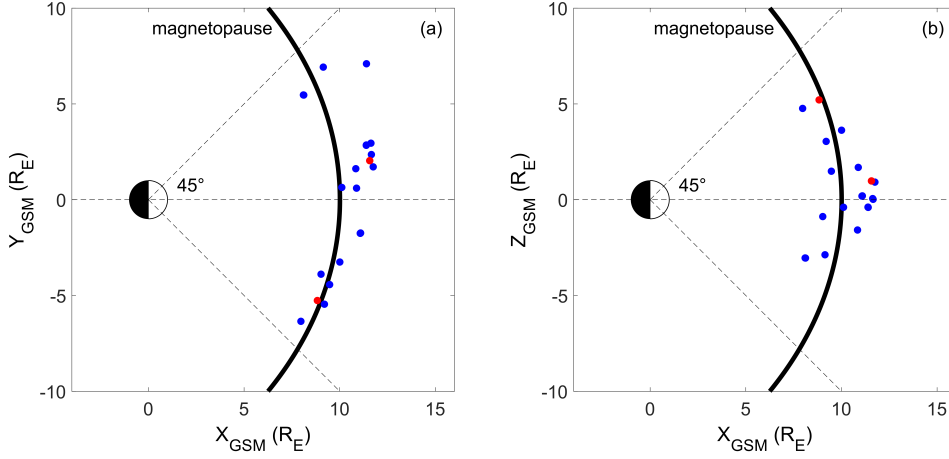


**Figure 1.** Locations of selected magnetopause crossings with fast cold ion motion as observed by MMS, which have been projected into the (a) X-Y and (b) X-Z planes in geocentric solar magnetospheric coordinates. The solid black lines represent the magnetopause, and the red dots show the location of two events detailed presented in Figure 2 and Figure 3.

119 Figure 1 shows locations of thirty selected MMS magnetopause crossings from 2015  
 120 to 2021. These crossings are approximately evenly distributed in the dawn and dusk sides  
 121 of the magnetopause, but have some north-south asymmetry as the apogee of MMS space-  
 122 craft precess northward in years. We also note that there is a seasonal bias in these events,  
 123 as MMS dayside magnetopause crossings occur primarily during the winter seasons of  
 124 the north hemisphere. This seasonal bias implies a bias in the dipole tilt angle. How-  
 125 ever, the dipole tilt angle could influence the cusp indentation more significantly, but has  
 126 little effects on the shape of the dayside magnetopause according to empirical models  
 127 (Shue et al., 1997; Lin et al., 2010). Therefore, this seasonal bias in this data set can be  
 128 ignored.

129 In the following sections, we will first present two events as indicated by red dots  
 130 in Figure 1 to show how fast cold ion motion is related to the magnetopause deforma-  
 131 tion, and then investigate the preferred solar wind conditions in a statistical view.

## 132 2.1 Event study

133 Figure 2 provides an overview of the magnetopause crossing from the magnetosheath  
 134 to the magnetosphere on February 1, 2020. During this time interval, The MMS space-  
 135 craft are located approximately at (8.83 -5.26 5.21) R<sub>E</sub>. The magnetopause is charac-  
 136 terized by a large variation of the magnetic field ( $\Delta B_Z > 50$  nT, Figure 2a), high asym-  
 137 metry of plasma density (Figure 2c) and temperature (Figure 2e) and the appearance  
 138 of high-energy ions at the magnetospheric side ( $W_i > 10$  keV, Figure 2f). Meanwhile,  
 139 there are some unusual features during this magnetopause crossing. Comparing to the  
 140 plasma flows in the magnetosheath, which are diverted at the magnetopause with a speed  
 141 less than  $200 \text{ km s}^{-1}$ , the plasmas just inside the magnetopause are not idle, which have  
 142 a speed larger than the magnetosheath plasmas, primarily flowing sunward (Figure 2d).  
 143 Correspondingly, the measured electric field is extremely large inside the magnetopause,  
 144 reaching to  $\sim 15 \text{ mV m}^{-1}$  (Figure 2b). The related flow energy of the  $\mathbf{E} \times \mathbf{B}$  drift speed  
 145 is overplotted in Figure 2f, which varies with an cold ion population, except for some spin  
 146 effect. This indicates that cold ions may be responsible for this large speed plasma motion.  
 147 Figure 2n presents a 2D slice of ion velocity distributions in the  $\mathbf{V}_{\mathbf{E} \times \mathbf{B}} - \mathbf{V}_B$  plane

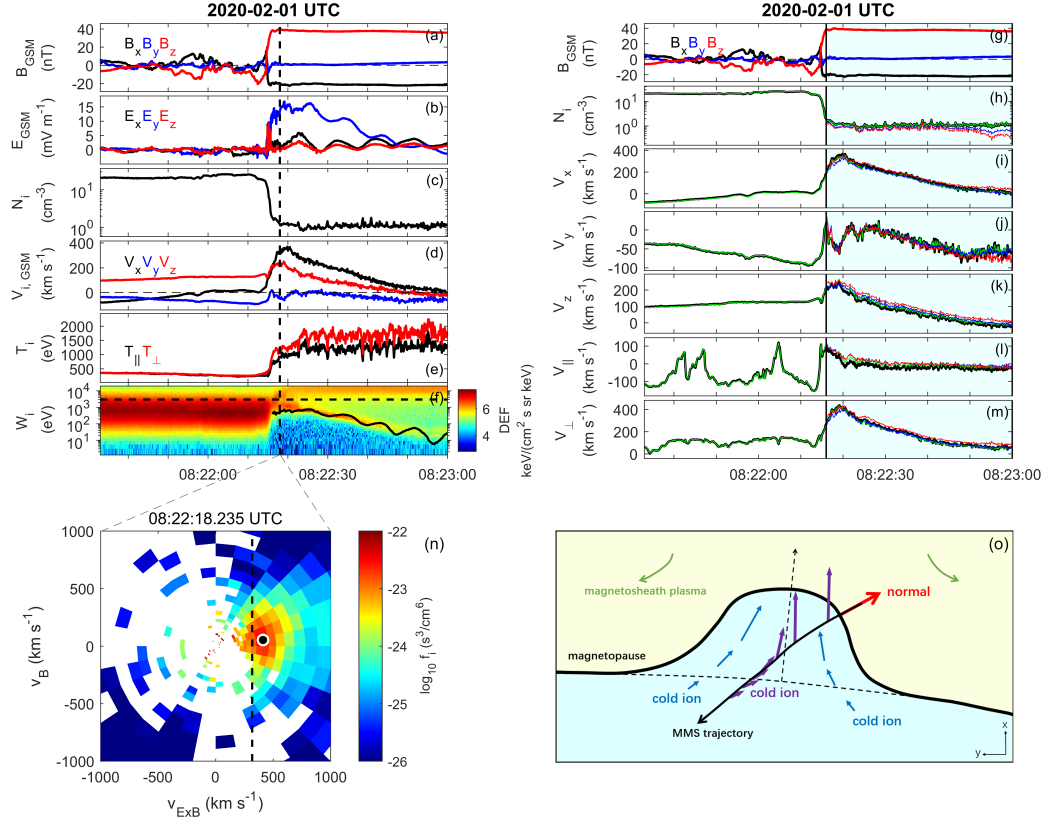


**Figure 2.** An overview of the magnetopause crossing on February 1, 2020. Panels at the left side show (a) magnetic field, (b) electric field, (c) ion number density, (d) ion velocity, (e) ion temperature, and (f) ion omnidirectional energy flux. Panels at the right side show (g) magnetic field, (h) the recalculated ion number density, and (i - m) the recalculated ion speed at different directions. The black curves represent the published data, and the green curves show the recalculated ion moments from velocity distributions. The partial cold ion moments are presented in blue and red curves, and the methods can be found in the context. (n) A two-dimensional slice of the ion velocity distribution at the time indicated by the vertical black line in panels (a - f). The dotted line in panel (n) indicates the electric drift speed, and the filled black dot shows the ion bulk speed. (o) A cartoon of the magnetopause deformation in this event. The magnetosheath and magnetosphere are displayed in yellow and cyan, and green and blue arrows indicate possible plasma flows in these two regions. The solid black arrow indicates the MMS trajectory during the magnetopause crossing and purple arrows show the observed cold ion velocities along MMS trajectory. The dotted black arrow and the red arrow are the predicted and observed magnetopause normal directions.

148 just inside the magnetopause (marked by the vertical dotted line in Figure 2a - 2f), in  
 149 which we can find a relatively cold ion population that flows with a  $E \times B$  speed (indi-  
 150 cated by the dotted black line). This result is consistent with the frozen-in nature of cold  
 151 ions, and magnetic flux tubes move with these cold ions at the magnetopause.

152 To further confirm these observations, we calculate the cold ion moments in dif-  
 153 ferent ways. First, we integrate the ion moments from measured velocity distributions  
 154 (the green curves in Figure 2h - 2m), which are nearly identical with published data (the  
 155 black curves). Then we separate the cold ion population, and calculate its partial mo-  
 156 ments dependently. The blue curves show the partial ion moments with energy lower than  
 157 3 keV (the horizontal line in Figure 2f), which exclude the high-energy magnetospheric  
 158 ions, while the red ones present the results in a more careful way, which separates cold  
 159 ions in the velocity phase space (Li et al., 2017). Though the calculated cold ion den-  
 160 sities have some slight differences (Figure 2h), it clearly shows that cold ions are the ma-  
 161 jor component inside the magnetopause. Therefore, the cold ion velocity is very simil-  
 162 ar to the velocity of all ions (Figure 2h - 2m). The maximum perpendicular speed of  
 163 cold ions is  $\sim 360 \text{ km s}^{-1}$  when reaching to the magnetopause, and the parallel speed  
 164 is relatively small. As cold ions are frozen-in with the magnetic field lines as shown above,  
 165 the question now is how to understand these large sunward cold ion flows. For exam-  
 166 ple, we should clarify these cold ions are flowing towards the magnetopause or moving  
 167 with the magnetopause.

168 The magnetopause properties are investigated here. The four spacecraft timing method  
 169 is applied to estimate the magnetopause normal direction and speed. It gives  $V_{TM} \sim$   
 170  $156 \times [0.49 -0.83 0.26] \text{ km s}^{-1}$  with estimated time delays from 08:22:14.20 to 08:22:16.00  
 171 UT. Using the same time interval, the magnetopause normal can be estimated based on  
 172 the maximum variance analysis (MVA) on the magnetic field, yielding to  $N_{MVA} = [0.47$   
 173  $-0.81 0.34]$ . The difference of magnetopause normals from these two methods is about  
 174  $6^\circ$ , indicating reliability of the results. However, using the upstream solar wind param-  
 175 eters from OMNI data:  $N_{sw} = 3.9 \text{ cm}^{-3}$ ,  $V_{sw} = [457 11 -14] \text{ km s}^{-1}$ , and  $B_{IMF} = [3.42$   
 176  $0.26 -0.17] \text{ nT}$ , we can obtain the modeled magnetopause normal from the empirical mag-  
 177 netopause model (Shue et al., 1997), showing  $N_{SH} = [0.88 -0.33 0.33]$ . A large deflection  
 178 of the magnetopause normal then can be found between the model and observations, reach-  
 179 ing to  $37^\circ$ . This indicates that the magnetopause is at least locally deformed. Meanwhile,  
 180 the magnetopause motion speed is much larger than its median value in statistics ( $\sim 40$   
 181  $\text{ km s}^{-1}$ , Paschmann et al., 2018), indicating fast outward motion of the magnetopause.  
 182 If we project the cold ion speed at the time close to the magnetopause to the normal di-  
 183 rection ( $V_{cold,N}$ , here we use the averaged normal flow speed from MVA and timing meth-  
 184 ods),  $V_{cold,N}$  roughly matches the magnetopause motion speed ( $\sim 156 \text{ km s}^{-1}$ , Table 1),  
 185 suggesting cold ions move with the magnetopause at a large speed. Figure 2o briefly sum-  
 186 maries this event: the magnetopause is locally deformed, and MMS crosses the deformed  
 187 magnetopause from one side, so that a large deflection of the magnetopause normal is  
 188 observed. This also explains why there is a large cold ion speed tangential to the nor-  
 189 mal direction ( $V_{cold,T}$ , Table 1), as cold ions primarily flow sunward.

190 The cold ion speed decreases gradually when MMS goes into the magnetosphere,  
 191 inferring MMS is moving away from the magnetopause. The distance between MMS space-  
 192 craft and the magnetopause is usually difficult to infer from in-situ measurements, but  
 193 we can get its lower limit here by integrating the cold ion speed, showing that the mag-  
 194 netopause has moved about  $1.3 R_E$  outward in 30 seconds. This result indicates that the  
 195 magnetopause is significantly deformed in this event, and fast cold ions can be taken as  
 196 a good indicator.

197 Figure 3 shows another magnetopause crossing event when MMS is located at  $[11.57$   
 198  $2.04 0.98] R_E$  on December 26, 2016. This event is in general similar to the first event,  
 199 showing fast cold ion motion exceeding  $400 \text{ km s}^{-1}$  just inside the magnetopause, but  
 200 this event also presents some different features. First, the sheath plasma flows have a

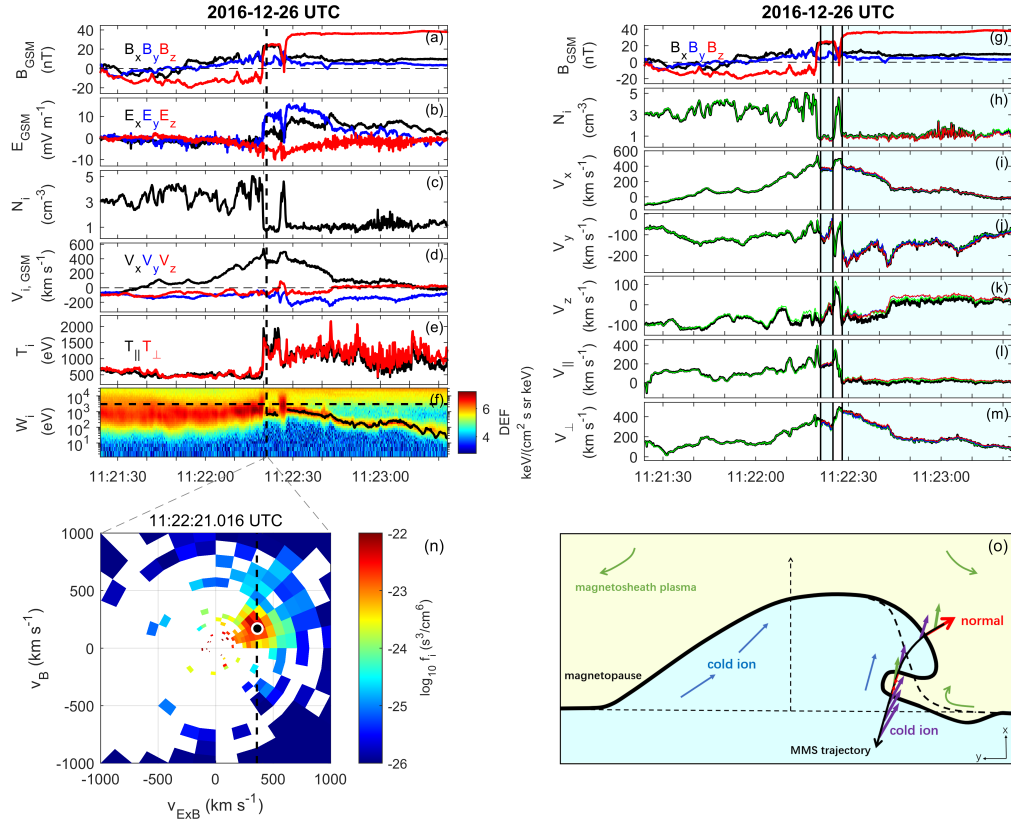


**Figure 3.** An overview of the magnetopause crossing on December 26, 2016. The figure format is similar to that in Figure 2.

**Table 1.** Magnetopause properties in Event 1 and 2.

Event	Time (UT)	Normal (Shue97)	$V_{MP}$ (Timing, km s <sup>-1</sup> )	Normal (Timing)	Normal (MVA)	$V_{cold,N}^a$ (km s <sup>-1</sup> )	$V_{cold,T}$ (km s <sup>-1</sup> )	Deflection angle (°)
1	20200201/ 08:22:14.91	[0.88 -0.33 0.33]	156	[0.49 -0.83 0.26]	[0.47 -0.81 0.34]	213	290	37
2	20161226/ 11:22:19.55	[0.99 0.12 0.06]	276	[0.41 -0.86 -0.32]	[0.41 -0.89 -0.19]	280	218	73
	20161226/ 11:22:26.96		380	[-0.80 0.36 0.48]	[-0.80 0.35 0.49]	315	65	134
	20161226/ 11:22:27.14		474	[0.95 -0.18 -0.26]	[0.95 -0.21 -0.23]	444	101	27

<sup>a</sup> This  $V_{cold,N}$  is the averaged value of the cold ion flow speed along the normal direction from the Timing and MVA method.

201 significant sunward component (Figure 3d). The speed of these sunward sheath plasma  
 202 flows increases when getting closed to the magnetopause, reaching to 540 km s<sup>-1</sup> just  
 203 in front of the magnetopause. These anomalous sunward sheath plasma flows are the op-  
 204 posite of the usual anti-sunward magnetosheath flows, which are believed to be closely  
 205 related with the magnetopause deformation as observed from THEMIS spacecraft (Shue  
 206 et al., 2009), and the magnetopause is under the rebound motion. Second, MMS cross  
 207 the magnetopause three times in 10 seconds. We check the magnetopause normal direc-  
 208 tion from these three magnetopause crossings from MMS, and find the magnetopause  
 209 is largely deformed (Table 1). In particular, during the second magnetopause crossing  
 210 from the magnetosphere to the sheath region, the sheath plasma keeps to move sunward,  
 211 indicating the magnetopause still moves outward. If we define the magnetopause nor-  
 212 mal always pointing towards the magnetosheath, deflection of the observed magnetopause  
 213 normal should be larger than 90° when comparing with empirical models (Figure 3o).  
 214 This suggests that some secondary magnetopause distortion is formed, and its spatial  
 215 scale is  $\sim 100$  km as the temporal separation of the last two magnetopause crossings is  
 216 only about 0.2 s. By comparison, we can infer the magnetopause shift by integrating the  
 217 cold ion motion, showing the magnetopause has at least moved outward for 2.5  $R_E$  in  
 218 60 seconds.

## 219 2.2 Statistics

220 Two MMS magnetopause crossing events with fast cold ion motion have been pre-  
 221 sented, showing the magnetopause is not stationary and has been largely deformed at  
 222 the same time. These observations suggest that fast-moving cold ions can be used as an  
 223 indicator of the magnetopause deformation, based on two arguments. First, due to the  
 224 frozen-in nature of cold ions, the magnetospheric magnetic flux should move with high-  
 225 speed cold ions, which is associated with fast magnetopause motion. Second, the observed  
 226 magnetopause normal is significantly deflected from the model predictions, indicating  
 227 the magnetopause is locally deformed. This result is also supported by the clear cold ion  
 228 flows tangential to the magnetopause (Table 1) and the gradual decrease of the cold ion  
 229 speed as MMS goes into the magnetosphere (Figures 2 and 3). In this section, we will  
 230 further examine these two arguments in a statistical view to investigate the relation be-  
 231 tween high-speed cold ions and the magnetopause deformation. To ensure the accuracy  
 232 of statistical results, we have further applied an additional criterion (The angle of mag-  
 233 netopause normals from the Timing and MVA methods is less than 15°) when select-  
 234 ing the magnetopause crossing events. Figure 4a shows a scatter plot of the observed mag-  
 235 netopause speed versus the cold ion speed normal to the local magnetopause in all 30  
 236 magnetopause crossings, in which the positive/negative sign of the cold ion speed indi-  
 237 cates the outward/inward magnetopause motion. A good linear relation between these  
 238 two parameters with a slope close to 1 is revealed, showing fast cold ion motion is ba-  
 239 sically comparable to the high-speed magnetopause motion. Some events with inward

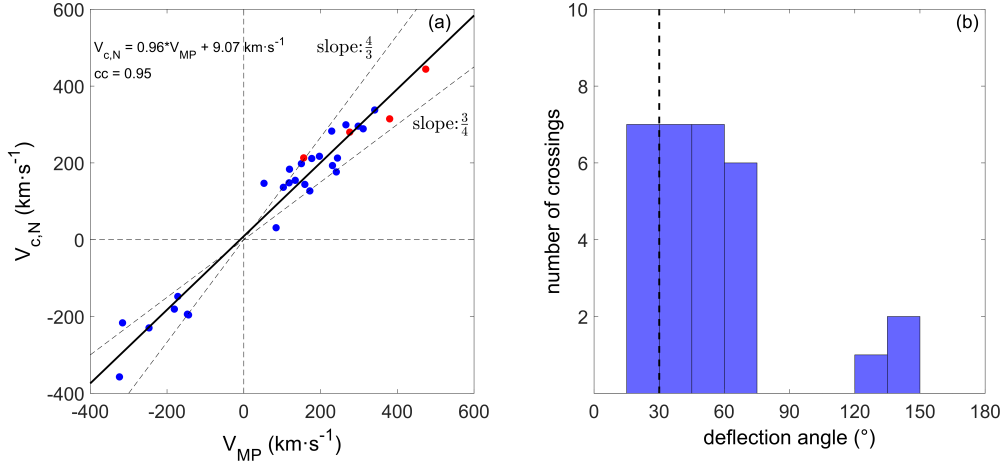


**Figure 4.** Statistics of the magnetopause crossings shown in Figure 1. (a) The scatter plot of the magnetopause’ speed ( $V_{MP}$ ) and the cold ion’s speed along the normal direction( $V_{c,N}$ ). The solid black line shows a linear fit of these two speeds. (b) Histogram of the deflection angles between the observed magnetopause normal and the prediction.

240 high-speed cold ions are also recorded, indicating the possible indentation of the mag-  
 241 netopause, but the event number is much fewer. Whether it suggests the earthward mag-  
 242 netopause motion is more difficult to reach a higher speed is not conclusive, as the event  
 243 set used in this study is relatively small. The cold ion speed normal to the local mag-  
 244 netopause sometimes is lower than  $200 \text{ km s}^{-1}$  (the threshold set for previous event se-  
 245 lection), and we attribute this to the local magnetopause deformation, which makes MMS  
 246 cross the magnetopause from one side. Figure 4b then displays the histogram of deflec-  
 247 tion angles between MMS observations and model predictions. We find the deflection  
 248 angle is usually larger than  $30^\circ$  in most magnetopause crossings, which is sufficiently larger  
 249 than uncertainties of magnetopause normal directions ( $15^\circ$ ), and thus it indicates the  
 250 magnetopause deformation is common when high-speed cold ions are present at the mag-  
 251 netopause. The deflection angles are larger than  $90^\circ$  in three cases, which are explained  
 252 by secondary magnetopause structures as shown in Figure 3.

253 By integrating the cold ion speed along the MMS trajectory, we can estimate the  
 254 amplitude of magnetopause deformation from in situ measurements as shown above. Here,  
 255 if we combine successive magnetopause crossings (i.e. the three magnetopause crossings  
 256 in the second case) into one event, 18 events are left from the total 30 magnetopause cross-  
 257 ings. Figure 5 presents that the related magnetopause deformation amplitude of these  
 258 events, which varies from  $0.2 R_E$  to  $\sim 2.5 R_E$ , and the meridian value is be approximately  
 259  $1.2 R_E$ . We note that the magnetopause deformation amplitude calculated from the cold  
 260 ion motion could be underestimated, but this result still indicates that the magnetopause  
 261 is significantly deformed with the presence of high-speed cold ions. And fast-moving cold  
 262 ions provide an applicable way to infer the magnetopause deformations.

263 Although we have shown fast-moving cold ions can be taken as an indicator of the  
 264 magnetopause deformation, the observation of cold ions are locally at the magnetopause,  
 265 meaning what causes the magnetopause deformation in the upstream solar wind is still  
 266 unknown. Here, we check the occurrence of above 18 fast-moving cold ion events under  
 267 different interplanetary magnetic field (IMF) cone angles (the angle between the IMF  
 268 direction and the Sun-Earth line). Figure 6a shows that these events recorded prefer to  
 269 occur under quasi-radial IMF conditions, and can be hardly found when IMF cone an-

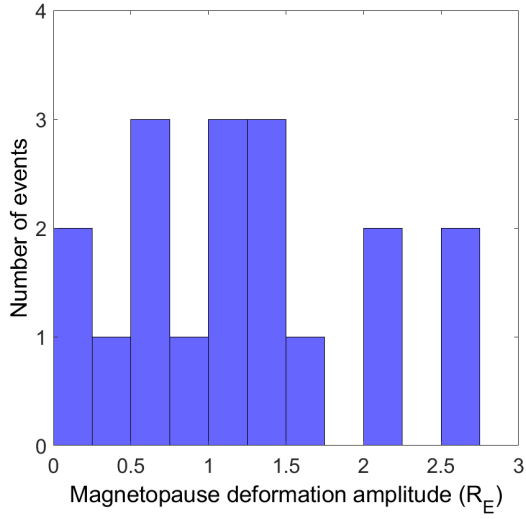


**Figure 5.** Statistics of magnetopause deformation amplitude of 18 magnetopause crossing events by integrating the cold ion speed.

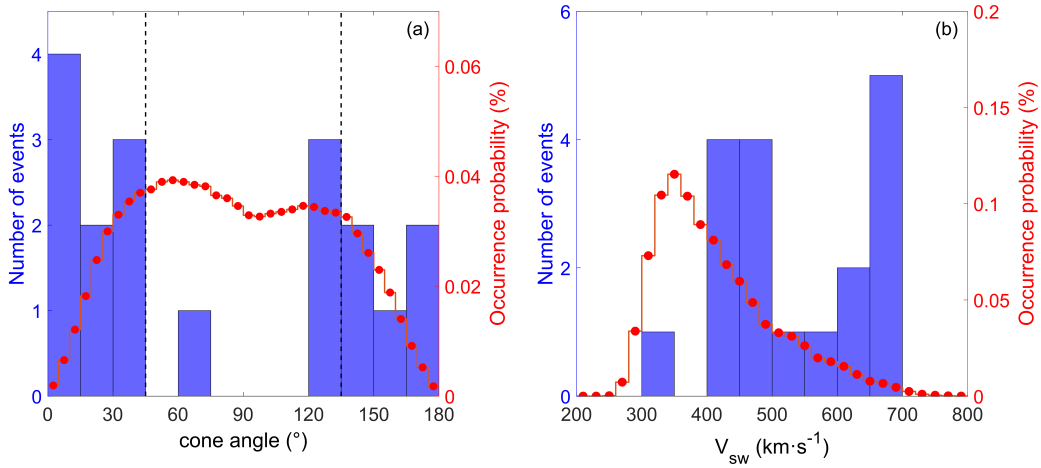


**Figure 6.** Statistics of related upstream solar wind conditions for the selected magnetopause crossing events. Panels show the number of events under (a) different IMF cone angles (the angle between the IMF direction and the Sun-Earth line) and (b) different solar wind speeds. The red lines show the occurrence probability of different IMF cone angles (a) and solar wind speeds (b) during MMS dayside magnetopause seasons from 2015 to 2021.

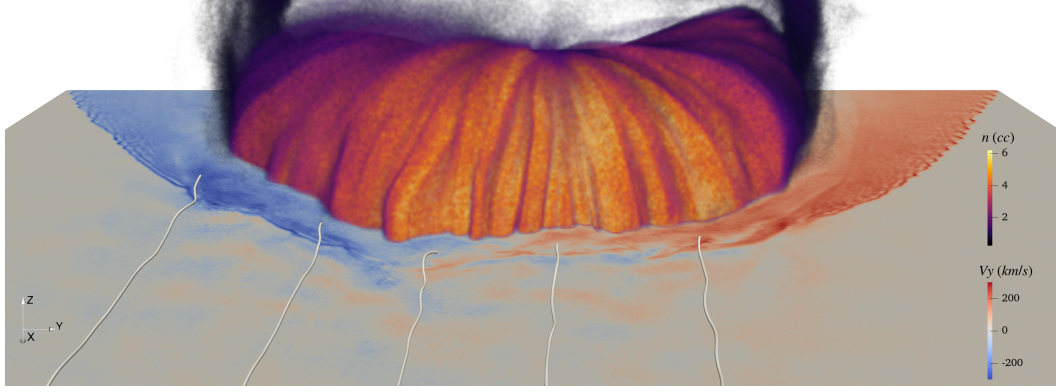


**Figure 7.** Magnetopause deformation from a 3-D global hybrid simulation under quasi-radial IMF condition. Several upstream IMF field lines are traced. The magnetopause location is estimated by the envelope of the 3-D density profile of ions trapped in the magnetosphere. A slice of solar wind ion bulk speed  $V_y$  is also plotted for reference.

270 gle is around  $90^\circ$ . To exclude the possible effect of the occurrence probability of the IMF  
 271 cone angles, we calculate the IMF cone angle occurrence during MMS dayside magne-  
 272 topause seasons from 2015 to 2021 (the red curve in Figure 6a). The result agrees well  
 273 with Parker spirals, showing the peak occurrence is at cone angles around  $45^\circ$  and  $135^\circ$ .  
 274 Therefore, 9 of 18 recorded events in Figure 6a that are found at cone angles  $< 30^\circ$  or  
 275  $> 150^\circ$  is not due to the uneven IMF cone angle effect, as the related occurrence prob-  
 276 ability of IMF cone angles is only 16.55%. Similarly, these events tend to occur under  
 277 higher solar wind conditions ( $V_{sw} > 400 \text{ km s}^{-1}$ , Figure 6b). This tendency is also dif-  
 278 ferent with the solar wind speed distributions, which peaks at  $V_{sw} \sim 350 \text{ km s}^{-1}$ .

279 As the fast-moving cold ions are locally observed by MMS at the magnetopause,  
 280 their dependence on solar wind conditions is somewhat unexpected. Here we try to ex-  
 281 plore the possible relations between them. First, the quasi-parallel bow shock shifts to  
 282 the nose region if the IMF cone angle is close to  $0^\circ$  or  $180^\circ$ , which would lead to a more  
 283 turbulent environment extending to the upstream foreshock region and downstream mag-  
 284 netosheath. The high-speed magnetosheath jets with local dynamic pressure enhance-  
 285 ment are then more frequently observed downstream of the quasi-parallel bow shock (Plaschke  
 286 et al., 2018). These high-speed jets under fast solar wind conditions are more likely to  
 287 pass through the magnetosheath and impact the magnetopause (LaMoury et al., 2021).  
 288 As the typical size of a high-speed jet varies from  $0.1 R_E$  to  $1 R_E$  (Plaschke et al., 2016,  
 289 2020), the related magnetopause deformation is temporally and spatially limited, which  
 290 results into fast magnetopause motion. Due to frozen-in nature of cold ions, they would  
 291 therefore get a high speed, if they can appear at the magnetopause. Thus, this explains  
 292 why fast-moving cold ions can be taken as an indicator of the magnetopause deforma-  
 293 tion. Figure 7 presents the local magnetopause deformation in a 3-D global hybrid sim-  
 294 ulation under quasi-radial IMF conditions (Yang et al., 2024), consistent with the pro-  
 295 cess described above.

### 296 3 Summary

297 In this study, we have shown that cold ions at the magnetopause can sometimes  
 298 reach to several hundreds of  $\text{km s}^{-1}$ , which are closely related to the magnetopause de-  
 299 formation from a statistical view. As the magnetopause deformation is not straightfor-  
 300 ward to be determined from in-situ measurements, this study suggests that fast-moving  
 301 cold ions can be taken as a useful tool to identify the magnetopause deformation. In ad-

302 dition, we also found fast-moving cold ions at the magnetopause are favorable to occur  
 303 when IMF is more flow-aligned and solar wind speed is higher. Therefore, we infer that  
 304 high-speed magnetosheath jets could be one direct cause of the MMS observations lo-  
 305 cally at the magnetopause, as they are more frequently to occur under similar solar wind  
 306 conditions. In other words, fast-moving cold ions are one direct consequence of the mag-  
 307 netopause impact of high-speed magnetosheath jets.

308 However, there are two things that should be further addressed. First, cold ions  
 309 do not appear at the magnetopause all the time, and they are not evenly distributed along  
 310 the magnetopause as well. So, although fast-moving cold ions can be taken as an indi-  
 311 cator for the magnetopause deformation, not all magnetopause deformations are accom-  
 312 panied with cold ions. Due to the dawn-dusk asymmetry of cold ion appearance at the  
 313 magnetopause, it is difficult to investigate if there are more magnetopause deformation  
 314 events at dawn-side magnetopause, which is downstream of the quasi-parallel bow shock  
 315 under the average Parker spirals. Second, the solar wind conditions are limited to be rel-  
 316 atively stable in this study, which is of course good to reveal the relation between up-  
 317 stream solar winds and the local magnetopause processes. But the solar wind transient  
 318 structures, such as HFAs, can also impact the magnetopause, leading to magnetopause  
 319 perturbations. In fact, fast-moving cold ions have been observed in an extreme magne-  
 320 topause motion event caused by an HFA (Jacobsen et al., 2009).

321 In general, fast-moving cold ions provide a new perspective to study the magne-  
 322 topause response to the solar wind from in-situ measurements. The forthcoming Solar  
 323 wind Magnetosphere Ionosphere Link Explorer (SMILE) mission aims to image the mag-  
 324 netopause with soft X-rays (C. Wang & Branduardi-Raymont, 2018; Branduardi-Raymont  
 325 et al., 2018). If time series of magnetopause images are able to distinguish the local mag-  
 326 netopause deformation, some relevant joint studies can be performed between the global  
 327 magnetopause images and the in-situ magnetopause crossings in the future.

## 328 Open Research Section

329 MMS data are available at the MMS Science Data Center (<https://lasp.colorado.edu/mms/sdc/public/about/browse-wrapper/>), and the solar wind data are acces-  
 330 sible at the CDAweb (<https://cdaweb.gsfc.nasa.gov/pub/data/>). The IRFU-Matlab  
 331 package (<https://github.com/irfu/irfu-matlab>) is used for data analysis. The mag-  
 332 netopause crossing list used in this study can be found at <https://zenodo.org/records/8283060>.  
 333  
 334

## 335 Acknowledgments

336 This work was supported by the National Key R&D Program of China (2021YFA0718600),  
 337 the National Natural Science Foundation of China (grants 42188101, 42122032, 41974196,  
 338 42274211, and 41974170) and the Specialized Research Fund for State Key Laborato-  
 339 ries of China.

## 340 References

- 341 André, M., & Cully, C. M. (2012). Low-energy ions: A previously hidden solar sys-  
 342 tem particle population. *Geophysical Research Letters*, *39*(3).  
 343 Branduardi-Raymont, G., Wang, C., Escoubet, C. P., Adamovic, M., Agnolon, D.,  
 344 Berthomier, M., . . . Zhu, Z. (2018). *SMILE definition study report* (V1.0 ed.;  
 345 Tech. Rep.). ESA/SCI. doi: 10.5270/esa.smile.definition.study\_report-2018-12  
 346 Dmitriev, A., Suvorova, A., & Chao, J.-K. (2011). A predictive model of geosyn-  
 347 chronous magnetopause crossings. *Journal of Geophysical Research: Space*  
 348 *Physics*, *116*(A5). doi: 10.1029/2010JA016208  
 349 Ergun, R., Tucker, S., Westfall, J., Goodrich, K., Malaspina, D., Summers, D., . . .

- 350 others (2016). The axial double probe and fields signal processing for the MMS  
 351 mission. *Space Science Reviews*, 199(1-4), 167–188.
- 352 Escoubet, C. P., Hwang, K.-J., Toledo-Redondo, S., Turc, L., Haaland, S., Aunai,  
 353 N., ... others (2020). Cluster and MMS simultaneous observations of magne-  
 354 tosheath high speed jets and their impact on the magnetopause. *Frontiers in*  
 355 *Astronomy and Space Sciences*, 78.
- 356 Fairfield, D. H. (1971). Average and unusual locations of the Earth's magnetopause  
 357 and bow shock. *Journal of Geophysical Research (1896-1977)*, 76(28), 6700–  
 358 6716. doi: 10.1029/JA076i028p06700
- 359 Hietala, H., Phan, T., Angelopoulos, V., Oieroset, M., Archer, M. O., Karlsson, T.,  
 360 & Plaschke, F. (2018). In situ observations of a magnetosheath high-speed jet  
 361 triggering magnetopause reconnection. *Geophysical Research Letters*, 45(4),  
 362 1732–1740.
- 363 Jacobsen, K., Phan, T., Eastwood, J., Sibeck, D., Moen, J., Angelopoulos, V., ...  
 364 others (2009). Themis observations of extreme magnetopause motion caused  
 365 by a hot flow anomaly. *Journal of Geophysical Research: Space Physics*,  
 366 114(A8).
- 367 Karimabadi, H., Roytershteyn, V., Vu, H., Omelchenko, Y., Scudder, J., Daughton,  
 368 W., ... others (2014). The link between shocks, turbulence, and magnetic  
 369 reconnection in collisionless plasmas. *Physics of Plasmas*, 21(6), 062308.
- 370 Katsavrias, C., Raptis, S., Daglis, I. A., Karlsson, T., Georgiou, M., & Balasis,  
 371 G. (2021). On the generation of Pi2 pulsations due to plasma flow pat-  
 372 terns around magnetosheath jets. *Geophysical Research Letters*, 48(15),  
 373 e2021GL093611.
- 374 LaMoury, A. T., Hietala, H., Plaschke, F., Vuorinen, L., & Eastwood, J. P. (2021).  
 375 Solar wind control of magnetosheath jet formation and propagation to the  
 376 magnetopause. *Journal of Geophysical Research: Space Physics*, 126(9),  
 377 e2021JA029592.
- 378 Li, W. Y., André, M., Khotyaintsev, Y. V., Vaivads, A., Fuselier, S., Graham, D. B.,  
 379 ... others (2017). Cold ionospheric ions in the magnetic reconnection outflow  
 380 region. *Journal of Geophysical Research: Space Physics*, 122(10), 10–194.
- 381 Lin, R. L., Zhang, X. X., Liu, S. Q., Wang, Y. L., & Gong, J. C. (2010). A three-  
 382 dimensional asymmetric magnetopause model. *Journal of Geophysical Re-*  
 383 *search: Space Physics*, 115(A4). doi: 10.1029/2009JA014235
- 384 Lindqvist, P.-A., Olsson, G., Torbert, R., King, B., Granoff, M., Rau, D., ... others  
 385 (2016). The spin-plane double probe electric field instrument for MMS. *Space*  
 386 *Science Reviews*, 199(1-4), 137–165.
- 387 Liu, Z.-Q., Lu, J. Y., Wang, C., Kabin, K., Zhao, J. S., Wang, M., ... Zhao, M. X.  
 388 (2015). A three-dimensional high mach number asymmetric magnetopause  
 389 model from global MHD simulation. *Journal of Geophysical Research: Space*  
 390 *Physics*, 120(7), 5645–5666. doi: 10.1002/2014JA020961
- 391 Ng, J., Chen, L.-J., & Omelchenko, Y. (2021). Bursty magnetic reconnection at the  
 392 earth's magnetopause triggered by high-speed jets. *Physics of Plasmas*, 28(9).
- 393 Nguyen, G., Aunai, N., Michotte de Welle, B., Jeandet, A., Lavraud, B., & Fontaine,  
 394 D. (2022). Massive multi-mission statistical study and analytical modeling of  
 395 the Earth's magnetopause: 2. shape and location. *Journal of Geophysical Re-*  
 396 *search: Space Physics*, 127(1), e2021JA029774. doi: 10.1029/2021JA029774
- 397 Paschmann, G., Haaland, S., Phan, T., Sonnerup, B. Ö., Burch, J., Torbert, R., ...  
 398 others (2018). Large-scale survey of the structure of the dayside magnetopause  
 399 by MMS. *Journal of Geophysical Research: Space Physics*, 123(3), 2018–2033.
- 400 Phan, T. D., & Paschmann, G. (1996). Low-latitude dayside magnetopause and  
 401 boundary layer for high magnetic shear: 1. structure and motion. *Journal of*  
 402 *Geophysical Research: Space Physics*, 101(A4), 7801–7815.
- 403 Plaschke, F., Hietala, H., Angelopoulos, V., & Nakamura, R. (2016). Geoeffective  
 404 jets impacting the magnetopause are very common. *Journal of Geophysical Re-*

- 405 search: *Space Physics*, 121(4), 3240–3253.
- 406 Plaschke, F., Hietala, H., Archer, M., Blanco-Cano, X., Kajdič, P., Karlsson, T., ...  
 407 others (2018). Jets downstream of collisionless shocks. *Space Science Reviews*,  
 408 214, 1–77.
- 409 Plaschke, F., Hietala, H., & Vörös, Z. (2020). Scale sizes of magnetosheath jets.  
 410 *Journal of Geophysical Research: Space Physics*, 125(9), e2020JA027962.
- 411 Pollock, C., Moore, T., Jacques, A., Burch, J., Gliese, U., Saito, Y., ... others  
 412 (2016). Fast plasma investigation for magnetospheric multiscale. *Space Science*  
 413 *Reviews*, 199(1-4), 331–406.
- 414 Russell, C., Anderson, B., Baumjohann, W., Bromund, K., Dearborn, D., Fischer,  
 415 D., ... others (2016). The magnetospheric multiscale magnetometers. *Space*  
 416 *Science Reviews*, 199(1-4), 189–256.
- 417 Šafránková, J., Goncharov, O., Němeček, Z., Přech, L., & Sibeck, D. (2012). Asym-  
 418 metric magnetosphere deformation driven by hot flow anomaly (ies). *Geophysic-*  
 419 *cal research letters*, 39(15).
- 420 Schwartz, S. J., Paschmann, G., Sckopke, N., Bauer, T. M., Dunlop, M., Fazaker-  
 421 ley, A. N., & Thomsen, M. F. (2000). Conditions for the formation of hot  
 422 flow anomalies at Earth’s bow shock. *Journal of Geophysical Research: Space*  
 423 *Physics*, 105(A6), 12639–12650.
- 424 Shue, J.-H., Chao, J., Fu, H., Russell, C., Song, P., Khurana, K., & Singer, H.  
 425 (1997). A new functional form to study the solar wind control of the mag-  
 426 netopause size and shape. *Journal of Geophysical Research: Space Physics*,  
 427 102(A5), 9497–9511.
- 428 Shue, J.-H., Chao, J.-K., Song, P., McFadden, J., Suvorova, A., Angelopoulos, V.,  
 429 ... Plaschke, F. (2009). Anomalous magnetosheath flows and distorted sub-  
 430 solar magnetopause for radial interplanetary magnetic fields. *Geophysical*  
 431 *Research Letters*, 36(18).
- 432 Shue, J.-H., Song, P., Russell, C., Steinberg, J., Chao, J., Zastenker, G., ... others  
 433 (1998). Magnetopause location under extreme solar wind conditions. *Journal*  
 434 *of Geophysical Research: Space Physics*, 103(A8), 17691–17700.
- 435 Sibeck, D., Borodkova, N., Schwartz, S., Owen, C., Kessel, R., Kokubun, S., ...  
 436 others (1999). Comprehensive study of the magnetospheric response to a  
 437 hot flow anomaly. *Journal of Geophysical Research: Space Physics*, 104(A3),  
 438 4577–4593.
- 439 Sibeck, D., Kudela, K., Lepping, R., Lin, R., Nemecek, Z., Nozdrachev, M., ... oth-  
 440 ers (2000). Magnetopause motion driven by interplanetary magnetic field  
 441 variations. *Journal of Geophysical Research: Space Physics*, 105(A11), 25155–  
 442 25169.
- 443 Staples, F., Rae, I., Smith, A., Raymer, K., Case, N., Rodger, C., ... others (2020).  
 444 Do statistical models capture the dynamics of the magnetopause during sud-  
 445 den magnetospheric compressions? *Journal of Geophysical Research: Space*  
 446 *Physics*, 125(4), e2019JA027289.
- 447 Toledo-Redondo, S., André, M., Aunai, N., Chappell, C. R., Dargent, J., Fuselier,  
 448 S., ... others (2021). Impacts of ionospheric ions on magnetic reconnec-  
 449 tion and earth’s magnetosphere dynamics. *Reviews of Geophysics*, 59(3),  
 450 e2020RG000707.
- 451 Toledo-Redondo, S., André, M., Vaivads, A., Khotyaintsev, Y. V., Lavraud, B.,  
 452 Graham, D. B., ... Aunai, N. (2016). Cold ion heating at the dayside mag-  
 453 netopause during magnetic reconnection. *Geophysical Research Letters*, 43(1),  
 454 58–66.
- 455 Wang, B., Nishimura, Y., Hietala, H., Lyons, L., Angelopoulos, V., Plaschke, F.,  
 456 ... Weatherwax, A. (2018). Impacts of magnetosheath high-speed jets on  
 457 the magnetosphere and ionosphere measured by optical imaging and satel-  
 458 lite observations. *Journal of Geophysical Research: Space Physics*, 123(6),  
 459 4879–4894.

- 460 Wang, C., & Branduardi-Raymont, G. (2018). Progress of solar wind magnetosphere  
461 ionosphere link explorer(SMILE) mission. *Chinese Journal of Space Science*,  
462 *38*(5), 657–661.
- 463 Wang, X., Lu, J., Wang, M., Zhou, Y., & Hao, Y. (2023). Simultaneous observation  
464 of magnetopause expansion under radial imf and indentation by hsj. *Geophysical*  
465 *Research Letters*, *50*(20), e2023GL105270.
- 466 Xu, Q., Tang, B., Sun, T., Li, W., Zhang, X., Wei, F., ... Wang, C. (2022). Mod-  
467 eling of the subsolar magnetopause motion under interplanetary magnetic field  
468 southward turning. *Space Weather*, *20*(12), e2022SW003250.
- 469 Yang, Z., Jarvinen, R., Guo, X., Sun, T., Koutroumpa, D., Parks, G., ... Wang, C.  
470 (2024). Deformations at Earth's dayside magnetopause during quasi-radial  
471 IMF conditions: Global kinetic simulations and soft X-ray imaging. *Earth and*  
472 *Planetary Physics*, *8*. doi: 10.26464/epp2023059
- 473 Zhang, H., Zong, Q., Connor, H., Delamere, P., Facskó, G., Han, D., ... others  
474 (2022). Dayside transient phenomena and their impact on the magnetosphere  
475 and ionosphere. *Space Science Reviews*, *218*(5), 40.

# The magnetopause deformation indicated by fast cold ion motion

Wenlong Guo<sup>1</sup>, Binbin Tang<sup>2</sup>, Qinghe Zhang<sup>1</sup>, Wenya Li<sup>2</sup>, Zhongwei Yang<sup>2</sup>,  
Tianran Sun<sup>2</sup>, Jiuqi Ma<sup>3</sup>, Xiaoxin Zhang<sup>4</sup>, Xiaocheng Guo<sup>2</sup>, and Chi Wang<sup>2</sup>

<sup>1</sup>Shandong Provincial Key Laboratory of Optical Astronomy and Solar-Terrestrial Environment, Institute of Space Sciences, Shandong University, Weihai, China.

<sup>2</sup>State Key Laboratory of Space Weather, National Space Science Center, Chinese Academy of Sciences, Beijing, China.

<sup>3</sup>School of Earth and Space Sciences, University of Science and Technology of China, Hefei, China.

<sup>4</sup>Key Laboratory of Space Weather, National Center for SpaceWeather, China Meteorological Administration, Beijing, China.

## Key Points:

- The magnetopause is found to be significantly deformed with the presence of fast-moving cold ions, whose speed can exceed  $\sim 400 \text{ km s}^{-1}$ .
- The inferred magnetopause deformation amplitude varies from  $\sim 0.2$  to  $2.5 R_E$ .
- The observed magnetopause deformation prefers to occur under quasi-radial IMF and fast solar wind conditions.

---

Corresponding author: Binbin Tang and Qinghe Zhang, [bbtang@spaceweather.ac.cn](mailto:bbtang@spaceweather.ac.cn),  
[zhangqinghe@sdu.edu.cn](mailto:zhangqinghe@sdu.edu.cn)

## Abstract

The magnetopause deformation due to the upstream magnetosheath pressure perturbations is important to understand the solar wind - magnetosphere coupling process, but how to identify such events from in-situ spacecraft observations is still challenging. In this study, we investigate magnetopause crossing events with fast-moving cold ions in the magnetosphere from Magnetospheric Multiscale (MMS) observations, and find when fast-moving cold ions are present at the magnetopause, they are closely associated with the magnetopause deformation, which is featured by fast magnetopause motion and significant magnetopause normal deflection from model predictions. Therefore, fast-moving cold ions can be a useful indicator to search for magnetopause deformation events. By integrating the cold ion speed, the inferred magnetopause deformation amplitude varies from 0.2 to  $\sim 2.5 R_E$ . Further statistics indicate that such magnetopause deformation events prefer to occur under quasi-radial interplanetary magnetic field and fast solar wind conditions, suggesting high-speed magnetosheath jets could be one direct cause of magnetopause deformations.

## 1 Introduction

The magnetopause is a boundary that shields the Earth's magnetosphere from the shocked solar wind. Its size and configuration are acutely important when investigating interactions between the interplanetary and magnetospheric environments, as various processes, such as magnetic reconnection and surface waves, can occur at the magnetopause, enabling mass and energy transfer across it.

To a first-order approximation, the magnetopause can be effectively represented through empirical models on large scales. For example, its shape and location have been extensively functioned (e.g. Fairfield, 1971; Shue et al., 1997, 1998; Lin et al., 2010; Dmitriev et al., 2011; Liu et al., 2015; Nguyen et al., 2022), which helps researchers to gain a preliminary understanding of the magnetopause by providing a basic response of the magnetopause under different solar wind and magnetospheric conditions. The accuracy of some widely used empirical magnetopause models has been tested with a large database of in-situ spacecraft crossings (Staples et al., 2020). The result shows that the magnetopause model can be used to estimate magnetopause location to within  $\pm 1$  Earth radii ( $R_E$ ) for the majority of magnetopause crossing events (74%), but sometimes discrepancies between measurements and model predictions can be large. This discrepancy can be partly attributed to the non-stationary nature of the magnetopause, which moves and changes under varying upstream plasma and magnetic field conditions. It is found that the usual magnetopause motion speed along its normal direction is around  $40 \text{ km s}^{-1}$  from in-situ spacecraft measurements (e.g. Phan & Paschmann, 1996; Paschmann et al., 2018), and the global simulations get a similar result (Xu et al., 2022). However, sometimes the magnetopause can move extremely fast, reaching to a speed over  $200 \text{ km s}^{-1}$  (Phan & Paschmann, 1996; Paschmann et al., 2018). Such fast magnetopause motion should be probably caused by rapid pressure variations in the upstream magnetosheath. Actually, the magnetosheath is highly turbulent (Karimabadi et al., 2014), and structures with transient pressure perturbations, such as mirror-mode waves, high-speed magnetosheath jets (HSJs), and downstream propagating solar wind/foreshock transients, can frequently occur. Impacts of these structures to the magnetopause can be hardly incorporated into empirical models due to their transient nature, but many related event studies have been performed.

Sibeck et al. (1999) has shown that the pressure within a hot flow anomaly (HFA, one typical solar wind transient structure) can be depressed by an order in magnitude with respect to the ambient background, allowing the magnetopause move outward about  $5 R_E$  in 7 minutes during the impacting process. Such HFA impact to the magnetopause has been displayed in different events, which in general can lead into the fast magnetopause

69 compression and expansion (Sibeck et al., 2000; Jacobsen et al., 2009; Šafránková et al.,  
70 2012; Zhang et al., 2022). Similarly, HSJs with local pressure enhancements can induce  
71 obvious inward magnetopause motion, following by possible subsequent magnetopause  
72 rebound (Shue et al., 2009; Plaschke et al., 2018; X. Wang et al., 2023) and the observed  
73 magnetopause normal can significantly differ from model predictions (Escoubet et al.,  
74 2020). Accompanied with the magnetopause deformation, magnetic reconnection can be  
75 triggered at the magnetopause (Hietala et al., 2018; Ng et al., 2021), waves can be gen-  
76 erated in the magnetosphere (Katsavrias et al., 2021), and the ionosphere can have some  
77 response as well (B. Wang et al., 2018). Therefore, investigations of the magnetopause  
78 deformation caused by these pressure perturbation structures are very helpful to under-  
79 stand the solar wind-magnetosphere coupling process, as their occurrence rates are not  
80 rare (Plaschke et al., 2016; Schwartz et al., 2000). However, due to limited cross-sections  
81 of these structures (for example, the spatial scale of HSJs varies from  $\sim 0.1$  to  $>1 R_E$  (Plaschke  
82 et al., 2016, 2020)), the investigation of their impact to the magnetopause is still insuf-  
83 ficient, which can be attributed to the difficulty in tracing the magnetopause response  
84 from in-situ spacecraft measurements.

85 Cold ions of ionospheric origin are often present in the magnetosphere (André &  
86 Cully, 2012). Due to the frozen-in nature of cold ions, they usually convect with mag-  
87 netic field lines in the direction perpendicular to the magnetic field and they can be de-  
88 tected by on board particle instruments when cold ions get a relatively large bulk en-  
89 ergy to overcome the spacecraft potential. Frequently, cold ions can reach to the mag-  
90 netopause, and evolve into processes at the magnetopause, such as magnetic reconnection  
91 (Toledo-Redondo et al., 2016, 2021; Li et al., 2017). The cold ion speed at the mag-  
92 netopause is often tens of  $\text{km s}^{-1}$ . In this study, we show that the speed of cold ions can  
93 reach to several hundreds of  $\text{km s}^{-1}$ , which can be taken as a good indicator for mag-  
94 netopause deformation, and the detection of fast-moving cold ions can be a useful tool  
95 to search for magnetopause deformation events.

## 96 2 Observation

97 In this study, we investigate magnetopause crossing events accompanied with fast-  
98 moving cold ions from MMS observations. We use magnetic field data from the fluxgate  
99 magnetometer (Russell et al., 2016), electric field data from the electric field double probes  
100 (Ergun et al., 2016; Lindqvist et al., 2016), and particle data from the fast plasma in-  
101 vestigation (Pollock et al., 2016). Due to the small separation of four MMS spacecraft  
102 (typically only a few to tens of kilometers at the magnetopause), data from individual  
103 satellites appear almost identical, and we primarily present the data from MMS 1. Un-  
104 less otherwise stated, all vectors are presented in geocentric solar magnetospheric (GSM)  
105 coordinates.

106 We select relevant magnetopause crossing events semi-manually using following cri-  
107 teria. First, the location where MMS cross the magnetopause is within a cone angle of  
108  $45^\circ$  centered on the Sun-Earth line, allowing us to focus on events near the subsolar re-  
109 gion. Second, the speed of cold ions is larger than  $200 \text{ km s}^{-1}$ , and  $V_x$  should be the ma-  
110 jor component. Third, sometimes cold ions are difficult to identify before reaching to the  
111 magnetopause, as they can be either heated or mixed with other ion populations in the  
112 magnetopause boundary layer. We limit the time difference between clear cold ion sig-  
113 natures and the magnetopause crossing is less than 10 seconds, ensuring that the cold  
114 ion motion can be closely related to the magnetopause. Finally, the interplanetary mag-  
115 netic field from OMNI should be stable at least for 15 min surrounding the magnetopause  
116 crossing, excluding the impact of the solar wind structures (such as magnetic disconti-  
117 nuities) to the magnetopause. If there are data gaps in the OMNI data set, we use time-  
118 shifted ACE data instead.

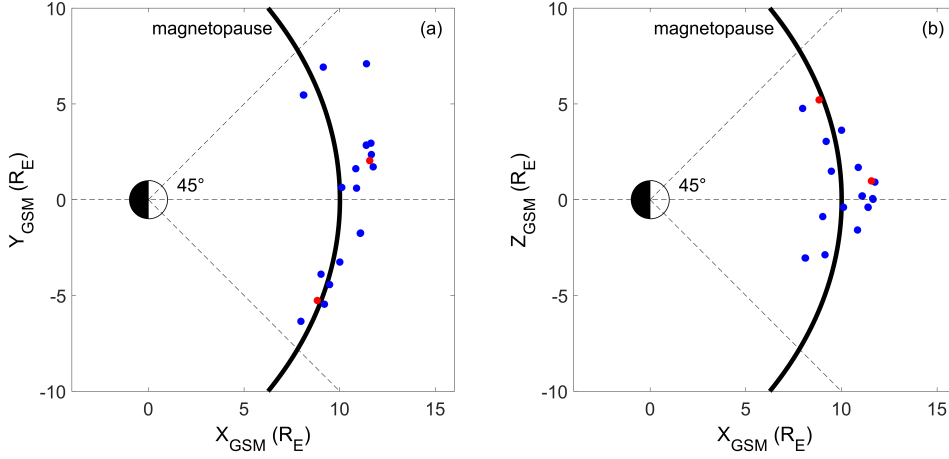


**Figure 1.** Locations of selected magnetopause crossings with fast cold ion motion as observed by MMS, which have been projected into the (a) X-Y and (b) X-Z planes in geocentric solar magnetospheric coordinates. The solid black lines represent the magnetopause, and the red dots show the location of two events detailed presented in Figure 2 and Figure 3.

119 Figure 1 shows locations of thirty selected MMS magnetopause crossings from 2015  
 120 to 2021. These crossings are approximately evenly distributed in the dawn and dusk sides  
 121 of the magnetopause, but have some north-south asymmetry as the apogee of MMS space-  
 122 craft precess northward in years. We also note that there is a seasonal bias in these events,  
 123 as MMS dayside magnetopause crossings occur primarily during the winter seasons of  
 124 the north hemisphere. This seasonal bias implies a bias in the dipole tilt angle. How-  
 125 ever, the dipole tilt angle could influence the cusp indentation more significantly, but has  
 126 little effects on the shape of the dayside magnetopause according to empirical models  
 127 (Shue et al., 1997; Lin et al., 2010). Therefore, this seasonal bias in this data set can be  
 128 ignored.

129 In the following sections, we will first present two events as indicated by red dots  
 130 in Figure 1 to show how fast cold ion motion is related to the magnetopause deforma-  
 131 tion, and then investigate the preferred solar wind conditions in a statistical view.

## 132 2.1 Event study

133 Figure 2 provides an overview of the magnetopause crossing from the magnetosheath  
 134 to the magnetosphere on February 1, 2020. During this time interval, The MMS space-  
 135 craft are located approximately at (8.83 -5.26 5.21) R<sub>E</sub>. The magnetopause is charac-  
 136 terized by a large variation of the magnetic field ( $\Delta B_Z > 50$  nT, Figure 2a), high asym-  
 137 metry of plasma density (Figure 2c) and temperature (Figure 2e) and the appearance  
 138 of high-energy ions at the magnetospheric side ( $W_i > 10$  keV, Figure 2f). Meanwhile,  
 139 there are some unusual features during this magnetopause crossing. Comparing to the  
 140 plasma flows in the magnetosheath, which are diverted at the magnetopause with a speed  
 141 less than  $200 \text{ km s}^{-1}$ , the plasmas just inside the magnetopause are not idle, which have  
 142 a speed larger than the magnetosheath plasmas, primarily flowing sunward (Figure 2d).  
 143 Correspondingly, the measured electric field is extremely large inside the magnetopause,  
 144 reaching to  $\sim 15 \text{ mV m}^{-1}$  (Figure 2b). The related flow energy of the  $\mathbf{E} \times \mathbf{B}$  drift speed  
 145 is overplotted in Figure 2f, which varies with an cold ion population, except for some spin  
 146 effect. This indicates that cold ions may be responsible for this large speed plasma motion.  
 147 Figure 2n presents a 2D slice of ion velocity distributions in the  $\mathbf{V}_{\mathbf{E} \times \mathbf{B}} - \mathbf{V}_B$  plane

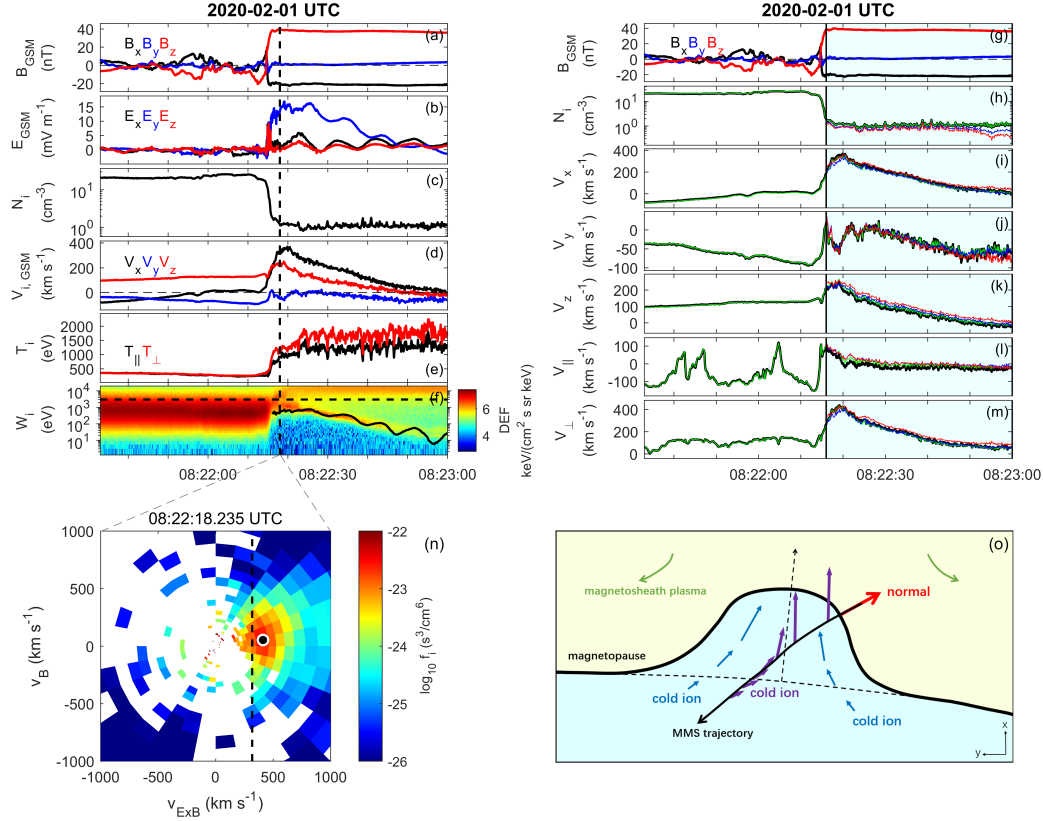


**Figure 2.** An overview of the magnetopause crossing on February 1, 2020. Panels at the left side show (a) magnetic field, (b) electric field, (c) ion number density, (d) ion velocity, (e) ion temperature, and (f) ion omnidirectional energy flux. Panels at the right side show (g) magnetic field, (h) the recalculated ion number density, and (i - m) the recalculated ion speed at different directions. The black curves represent the published data, and the green curves show the recalculated ion moments from velocity distributions. The partial cold ion moments are presented in blue and red curves, and the methods can be found in the context. (n) A two-dimensional slice of the ion velocity distribution at the time indicated by the vertical black line in panels (a - f). The dotted line in panel (n) indicates the electric drift speed, and the filled black dot shows the ion bulk speed. (o) A cartoon of the magnetopause deformation in this event. The magnetosheath and magnetosphere are displayed in yellow and cyan, and green and blue arrows indicate possible plasma flows in these two regions. The solid black arrow indicates the MMS trajectory during the magnetopause crossing and purple arrows show the observed cold ion velocities along MMS trajectory. The dotted black arrow and the red arrow are the predicted and observed magnetopause normal directions.

148 just inside the magnetopause (marked by the vertical dotted line in Figure 2a - 2f), in  
 149 which we can find a relatively cold ion population that flows with a  $E \times B$  speed (indi-  
 150 cated by the dotted black line). This result is consistent with the frozen-in nature of cold  
 151 ions, and magnetic flux tubes move with these cold ions at the magnetopause.

152 To further confirm these observations, we calculate the cold ion moments in dif-  
 153 ferent ways. First, we integrate the ion moments from measured velocity distributions  
 154 (the green curves in Figure 2h - 2m), which are nearly identical with published data (the  
 155 black curves). Then we separate the cold ion population, and calculate its partial mo-  
 156 ments dependently. The blue curves show the partial ion moments with energy lower than  
 157 3 keV (the horizontal line in Figure 2f), which exclude the high-energy magnetospheric  
 158 ions, while the red ones present the results in a more careful way, which separates cold  
 159 ions in the velocity phase space (Li et al., 2017). Though the calculated cold ion den-  
 160 sities have some slight differences (Figure 2h), it clearly shows that cold ions are the ma-  
 161 jor component inside the magnetopause. Therefore, the cold ion velocity is very simil-  
 162 ar to the velocity of all ions (Figure 2h - 2m). The maximum perpendicular speed of  
 163 cold ions is  $\sim 360 \text{ km s}^{-1}$  when reaching to the magnetopause, and the parallel speed  
 164 is relatively small. As cold ions are frozen-in with the magnetic field lines as shown above,  
 165 the question now is how to understand these large sunward cold ion flows. For exam-  
 166 ple, we should clarify these cold ions are flowing towards the magnetopause or moving  
 167 with the magnetopause.

168 The magnetopause properties are investigated here. The four spacecraft timing method  
 169 is applied to estimate the magnetopause normal direction and speed. It gives  $V_{TM} \sim$   
 170  $156 \times [0.49 \ -0.83 \ 0.26] \text{ km s}^{-1}$  with estimated time delays from 08:22:14.20 to 08:22:16.00  
 171 UT. Using the same time interval, the magnetopause normal can be estimated based on  
 172 the maximum variance analysis (MVA) on the magnetic field, yielding to  $N_{MVA} = [0.47$   
 173  $-0.81 \ 0.34]$ . The difference of magnetopause normals from these two methods is about  
 174  $6^\circ$ , indicating reliability of the results. However, using the upstream solar wind param-  
 175 eters from OMNI data:  $N_{sw} = 3.9 \text{ cm}^{-3}$ ,  $V_{sw} = [457 \ 11 \ -14] \text{ km s}^{-1}$ , and  $B_{IMF} = [3.42$   
 176  $0.26 \ -0.17] \text{ nT}$ , we can obtain the modeled magnetopause normal from the empirical mag-  
 177 netopause model (Shue et al., 1997), showing  $N_{SH} = [0.88 \ -0.33 \ 0.33]$ . A large deflection  
 178 of the magnetopause normal then can be found between the model and observations, reach-  
 179 ing to  $37^\circ$ . This indicates that the magnetopause is at least locally deformed. Meanwhile,  
 180 the magnetopause motion speed is much larger than its median value in statistics ( $\sim 40$   
 181  $\text{ km s}^{-1}$ , Paschmann et al., 2018), indicating fast outward motion of the magnetopause.  
 182 If we project the cold ion speed at the time close to the magnetopause to the normal di-  
 183 rection ( $V_{cold,N}$ , here we use the averaged normal flow speed from MVA and timing meth-  
 184 ods),  $V_{cold,N}$  roughly matches the magnetopause motion speed ( $\sim 156 \text{ km s}^{-1}$ , Table 1),  
 185 suggesting cold ions move with the magnetopause at a large speed. Figure 2o briefly sum-  
 186 marizes this event: the magnetopause is locally deformed, and MMS crosses the deformed  
 187 magnetopause from one side, so that a large deflection of the magnetopause normal is  
 188 observed. This also explains why there is a large cold ion speed tangential to the nor-  
 189 mal direction ( $V_{cold,T}$ , Table 1), as cold ions primarily flow sunward.

190 The cold ion speed decreases gradually when MMS goes into the magnetosphere,  
 191 inferring MMS is moving away from the magnetopause. The distance between MMS space-  
 192 craft and the magnetopause is usually difficult to infer from in-situ measurements, but  
 193 we can get its lower limit here by integrating the cold ion speed, showing that the mag-  
 194 netopause has moved about  $1.3 R_E$  outward in 30 seconds. This result indicates that the  
 195 magnetopause is significantly deformed in this event, and fast cold ions can be taken as  
 196 a good indicator.

197 Figure 3 shows another magnetopause crossing event when MMS is located at  $[11.57$   
 198  $2.04 \ 0.98] R_E$  on December 26, 2016. This event is in general similar to the first event,  
 199 showing fast cold ion motion exceeding  $400 \text{ km s}^{-1}$  just inside the magnetopause, but  
 200 this event also presents some different features. First, the sheath plasma flows have a

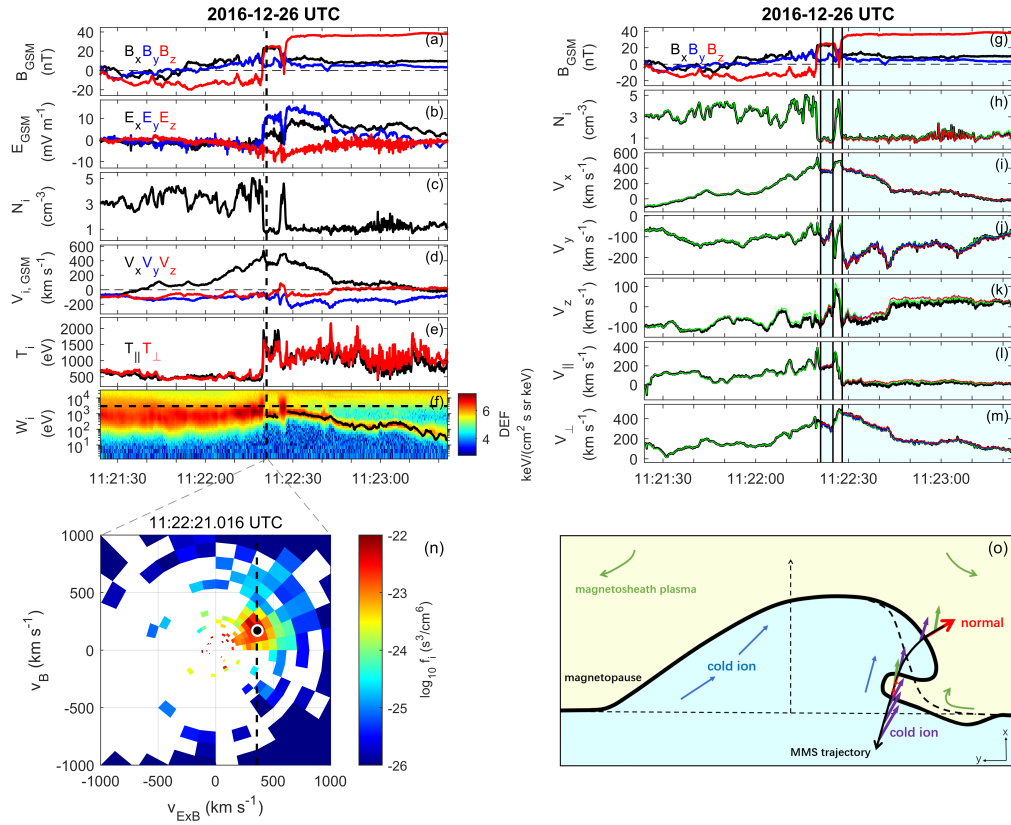


**Figure 3.** An overview of the magnetopause crossing on December 26, 2016. The figure format is similar to that in Figure 2.

**Table 1.** Magnetopause properties in Event 1 and 2.

Event	Time (UT)	Normal (Shue97)	$V_{MP}$ (Timing, km s <sup>-1</sup> )	Normal (Timing)	Normal (MVA)	$V_{cold,N}^a$ (km s <sup>-1</sup> )	$V_{cold,T}$ (km s <sup>-1</sup> )	Deflection angle (°)
1	20200201/ 08:22:14.91	[0.88 -0.33 0.33]	156	[0.49 -0.83 0.26]	[0.47 -0.81 0.34]	213	290	37
2	20161226/ 11:22:19.55	[0.99 0.12 0.06]	276	[0.41 -0.86 -0.32]	[0.41 -0.89 -0.19]	280	218	73
	20161226/ 11:22:26.96		380	[-0.80 0.36 0.48]	[-0.80 0.35 0.49]	315	65	134
	20161226/ 11:22:27.14		474	[0.95 -0.18 -0.26]	[0.95 -0.21 -0.23]	444	101	27

<sup>a</sup> This  $V_{cold,N}$  is the averaged value of the cold ion flow speed along the normal direction from the Timing and MVA method.

201 significant sunward component (Figure 3d). The speed of these sunward sheath plasma  
 202 flows increases when getting closed to the magnetopause, reaching to 540 km s<sup>-1</sup> just  
 203 in front of the magnetopause. These anomalous sunward sheath plasma flows are the op-  
 204 posite of the usual anti-sunward magnetosheath flows, which are believed to be closely  
 205 related with the magnetopause deformation as observed from THEMIS spacecraft (Shue  
 206 et al., 2009), and the magnetopause is under the rebound motion. Second, MMS cross  
 207 the magnetopause three times in 10 seconds. We check the magnetopause normal direc-  
 208 tion from these three magnetopause crossings from MMS, and find the magnetopause  
 209 is largely deformed (Table 1). In particular, during the second magnetopause crossing  
 210 from the magnetosphere to the sheath region, the sheath plasma keeps to move sunward,  
 211 indicating the magnetopause still moves outward. If we define the magnetopause nor-  
 212 mal always pointing towards the magnetosheath, deflection of the observed magnetopause  
 213 normal should be larger than 90° when comparing with empirical models (Figure 3o).  
 214 This suggests that some secondary magnetopause distortion is formed, and its spatial  
 215 scale is  $\sim 100$  km as the temporal separation of the last two magnetopause crossings is  
 216 only about 0.2 s. By comparison, we can infer the magnetopause shift by integrating the  
 217 cold ion motion, showing the magnetopause has at least moved outward for 2.5  $R_E$  in  
 218 60 seconds.

## 219 2.2 Statistics

220 Two MMS magnetopause crossing events with fast cold ion motion have been pre-  
 221 sented, showing the magnetopause is not stationary and has been largely deformed at  
 222 the same time. These observations suggest that fast-moving cold ions can be used as an  
 223 indicator of the magnetopause deformation, based on two arguments. First, due to the  
 224 frozen-in nature of cold ions, the magnetospheric magnetic flux should move with high-  
 225 speed cold ions, which is associated with fast magnetopause motion. Second, the observed  
 226 magnetopause normal is significantly deflected from the model predictions, indicating  
 227 the magnetopause is locally deformed. This result is also supported by the clear cold ion  
 228 flows tangential to the magnetopause (Table 1) and the gradual decrease of the cold ion  
 229 speed as MMS goes into the magnetosphere (Figures 2 and 3). In this section, we will  
 230 further examine these two arguments in a statistical view to investigate the relation be-  
 231 tween high-speed cold ions and the magnetopause deformation. To ensure the accuracy  
 232 of statistical results, we have further applied an additional criterion (The angle of mag-  
 233 netopause normals from the Timing and MVA methods is less than 15°) when select-  
 234 ing the magnetopause crossing events. Figure 4a shows a scatter plot of the observed mag-  
 235 netopause speed versus the cold ion speed normal to the local magnetopause in all 30  
 236 magnetopause crossings, in which the positive/negative sign of the cold ion speed indi-  
 237 cates the outward/inward magnetopause motion. A good linear relation between these  
 238 two parameters with a slope close to 1 is revealed, showing fast cold ion motion is ba-  
 239 sically comparable to the high-speed magnetopause motion. Some events with inward

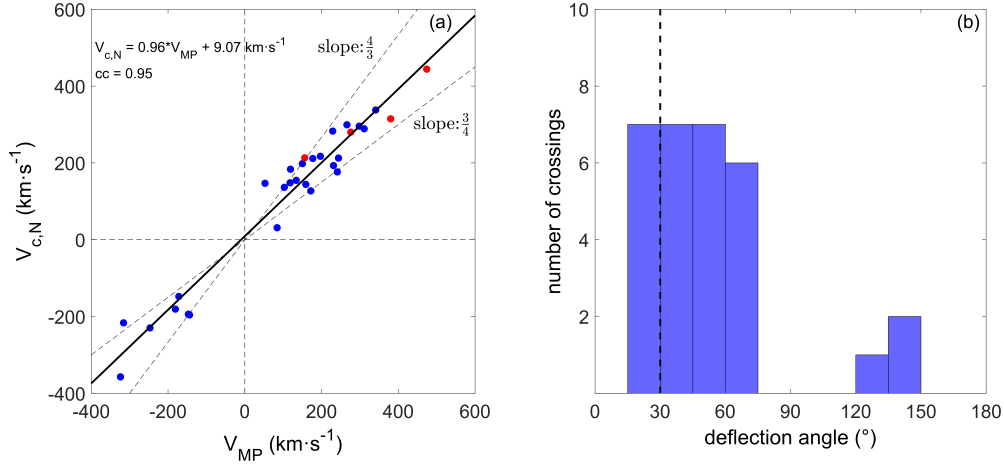


**Figure 4.** Statistics of the magnetopause crossings shown in Figure 1. (a) The scatter plot of the magnetopause’ speed ( $V_{MP}$ ) and the cold ion’s speed along the normal direction( $V_{c,N}$ ). The solid black line shows a linear fit of these two speeds. (b) Histogram of the deflection angles between the observed magnetopause normal and the prediction.

240 high-speed cold ions are also recorded, indicating the possible indentation of the mag-  
 241 netopause, but the event number is much fewer. Whether it suggests the earthward mag-  
 242 netopause motion is more difficult to reach a higher speed is not conclusive, as the event  
 243 set used in this study is relatively small. The cold ion speed normal to the local mag-  
 244 netopause sometimes is lower than  $200 \text{ km s}^{-1}$  (the threshold set for previous event se-  
 245 lection), and we attribute this to the local magnetopause deformation, which makes MMS  
 246 cross the magnetopause from one side. Figure 4b then displays the histogram of deflec-  
 247 tion angles between MMS observations and model predictions. We find the deflection  
 248 angle is usually larger than  $30^\circ$  in most magnetopause crossings, which is sufficiently larger  
 249 than uncertainties of magnetopause normal directions ( $15^\circ$ ), and thus it indicates the  
 250 magnetopause deformation is common when high-speed cold ions are present at the mag-  
 251 netopause. The deflection angles are larger than  $90^\circ$  in three cases, which are explained  
 252 by secondary magnetopause structures as shown in Figure 3.

253 By integrating the cold ion speed along the MMS trajectory, we can estimate the  
 254 amplitude of magnetopause deformation from in situ measurements as shown above. Here,  
 255 if we combine successive magnetopause crossings (i.e. the three magnetopause crossings  
 256 in the second case) into one event, 18 events are left from the total 30 magnetopause cross-  
 257 ings. Figure 5 presents that the related magnetopause deformation amplitude of these  
 258 events, which varies from  $0.2 R_E$  to  $\sim 2.5 R_E$ , and the meridian value is be approximately  
 259  $1.2 R_E$ . We note that the magnetopause deformation amplitude calculated from the cold  
 260 ion motion could be underestimated, but this result still indicates that the magnetopause  
 261 is significantly deformed with the presence of high-speed cold ions. And fast-moving cold  
 262 ions provide an applicable way to infer the magnetopause deformations.

263 Although we have shown fast-moving cold ions can be taken as an indicator of the  
 264 magnetopause deformation, the observation of cold ions are locally at the magnetopause,  
 265 meaning what causes the magnetopause deformation in the upstream solar wind is still  
 266 unknown. Here, we check the occurrence of above 18 fast-moving cold ion events under  
 267 different interplanetary magnetic field (IMF) cone angles (the angle between the IMF  
 268 direction and the Sun-Earth line). Figure 6a shows that these events recorded prefer to  
 269 occur under quasi-radial IMF conditions, and can be hardly found when IMF cone an-

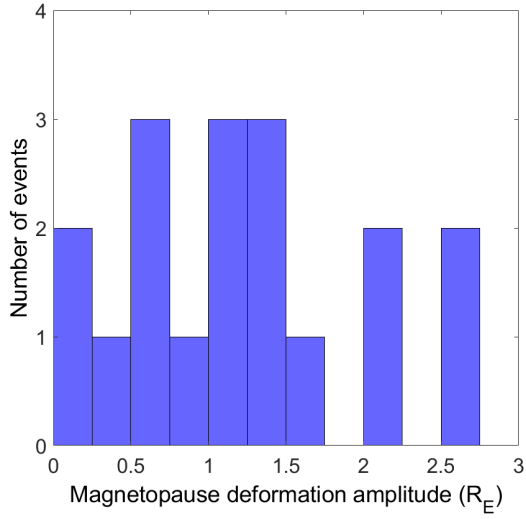


**Figure 5.** Statistics of magnetopause deformation amplitude of 18 magnetopause crossing events by integrating the cold ion speed.

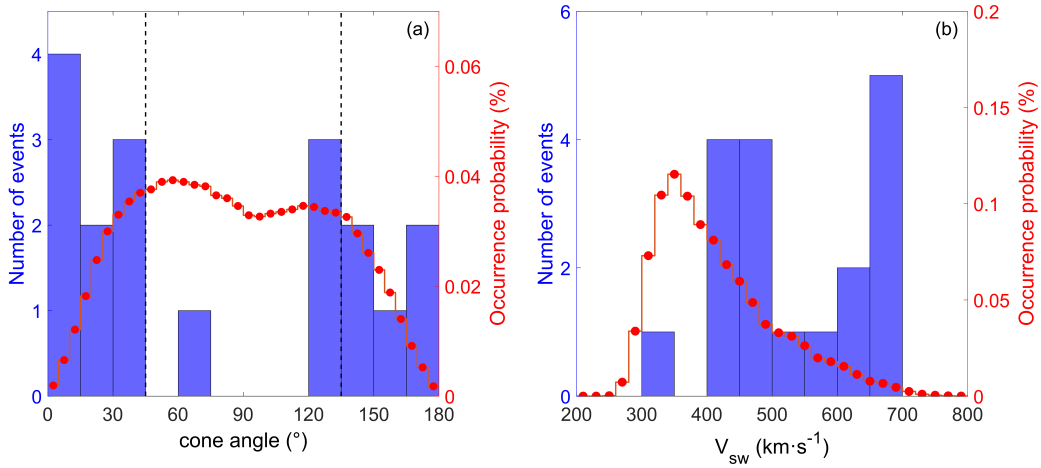


**Figure 6.** Statistics of related upstream solar wind conditions for the selected magnetopause crossing events. Panels show the number of events under (a) different IMF cone angles (the angle between the IMF direction and the Sun-Earth line) and (b) different solar wind speeds. The red lines show the occurrence probability of different IMF cone angles (a) and solar wind speeds (b) during MMS dayside magnetopause seasons from 2015 to 2021.

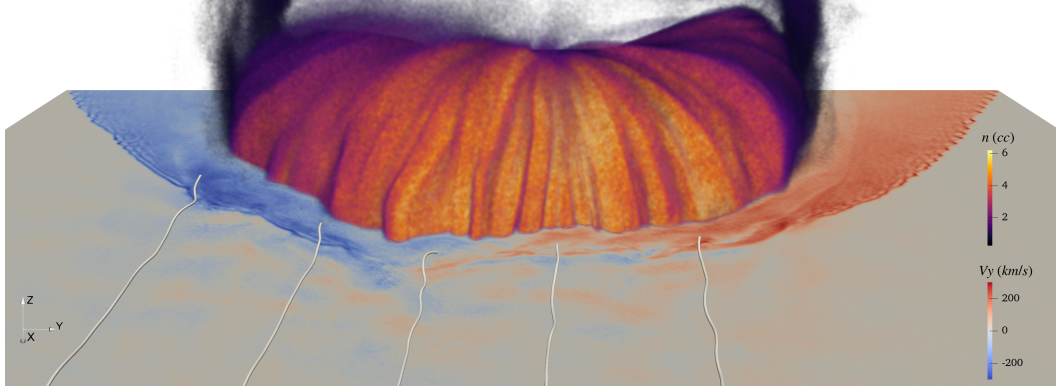


**Figure 7.** Magnetopause deformation from a 3-D global hybrid simulation under quasi-radial IMF condition. Several upstream IMF field lines are traced. The magnetopause location is estimated by the envelope of the 3-D density profile of ions trapped in the magnetosphere. A slice of solar wind ion bulk speed  $V_y$  is also plotted for reference.

270 gle is around  $90^\circ$ . To exclude the possible effect of the occurrence probability of the IMF  
 271 cone angles, we calculate the IMF cone angle occurrence during MMS dayside magne-  
 272 topause seasons from 2015 to 2021 (the red curve in Figure 6a). The result agrees well  
 273 with Parker spirals, showing the peak occurrence is at cone angles around  $45^\circ$  and  $135^\circ$ .  
 274 Therefore, 9 of 18 recorded events in Figure 6a that are found at cone angles  $< 30^\circ$  or  
 275  $> 150^\circ$  is not due to the uneven IMF cone angle effect, as the related occurrence prob-  
 276 ability of IMF cone angles is only 16.55%. Similarly, these events tend to occur under  
 277 higher solar wind conditions ( $V_{sw} > 400 \text{ km s}^{-1}$ , Figure 6b). This tendency is also dif-  
 278 ferent with the solar wind speed distributions, which peaks at  $V_{sw} \sim 350 \text{ km s}^{-1}$ .

279 As the fast-moving cold ions are locally observed by MMS at the magnetopause,  
 280 their dependence on solar wind conditions is somewhat unexpected. Here we try to ex-  
 281 plore the possible relations between them. First, the quasi-parallel bow shock shifts to  
 282 the nose region if the IMF cone angle is close to  $0^\circ$  or  $180^\circ$ , which would lead to a more  
 283 turbulent environment extending to the upstream foreshock region and downstream mag-  
 284 netosheath. The high-speed magnetosheath jets with local dynamic pressure enhance-  
 285 ment are then more frequently observed downstream of the quasi-parallel bow shock (Plaschke  
 286 et al., 2018). These high-speed jets under fast solar wind conditions are more likely to  
 287 pass through the magnetosheath and impact the magnetopause (LaMoury et al., 2021).  
 288 As the typical size of a high-speed jet varies from  $0.1 R_E$  to  $1 R_E$  (Plaschke et al., 2016,  
 289 2020), the related magnetopause deformation is temporally and spatially limited, which  
 290 results into fast magnetopause motion. Due to frozen-in nature of cold ions, they would  
 291 therefore get a high speed, if they can appear at the magnetopause. Thus, this explains  
 292 why fast-moving cold ions can be taken as an indicator of the magnetopause deforma-  
 293 tion. Figure 7 presents the local magnetopause deformation in a 3-D global hybrid sim-  
 294 ulation under quasi-radial IMF conditions (Yang et al., 2024), consistent with the pro-  
 295 cess described above.

### 296 3 Summary

297 In this study, we have shown that cold ions at the magnetopause can sometimes  
 298 reach to several hundreds of  $\text{km s}^{-1}$ , which are closely related to the magnetopause de-  
 299 formation from a statistical view. As the magnetopause deformation is not straightfor-  
 300 ward to be determined from in-situ measurements, this study suggests that fast-moving  
 301 cold ions can be taken as a useful tool to identify the magnetopause deformation. In ad-

302 dition, we also found fast-moving cold ions at the magnetopause are favorable to occur  
 303 when IMF is more flow-aligned and solar wind speed is higher. Therefore, we infer that  
 304 high-speed magnetosheath jets could be one direct cause of the MMS observations lo-  
 305 cally at the magnetopause, as they are more frequently to occur under similar solar wind  
 306 conditions. In other words, fast-moving cold ions are one direct consequence of the mag-  
 307 netopause impact of high-speed magnetosheath jets.

308 However, there are two things that should be further addressed. First, cold ions  
 309 do not appear at the magnetopause all the time, and they are not evenly distributed along  
 310 the magnetopause as well. So, although fast-moving cold ions can be taken as an indi-  
 311 cator for the magnetopause deformation, not all magnetopause deformations are accom-  
 312 panied with cold ions. Due to the dawn-dusk asymmetry of cold ion appearance at the  
 313 magnetopause, it is difficult to investigate if there are more magnetopause deformation  
 314 events at dawn-side magnetopause, which is downstream of the quasi-parallel bow shock  
 315 under the average Parker spirals. Second, the solar wind conditions are limited to be rel-  
 316 atively stable in this study, which is of course good to reveal the relation between up-  
 317 stream solar winds and the local magnetopause processes. But the solar wind transient  
 318 structures, such as HFAs, can also impact the magnetopause, leading to magnetopause  
 319 perturbations. In fact, fast-moving cold ions have been observed in an extreme magne-  
 320 topause motion event caused by an HFA (Jacobsen et al., 2009).

321 In general, fast-moving cold ions provide a new perspective to study the magne-  
 322 topause response to the solar wind from in-situ measurements. The forthcoming Solar  
 323 wind Magnetosphere Ionosphere Link Explorer (SMILE) mission aims to image the mag-  
 324 netopause with soft X-rays (C. Wang & Branduardi-Raymont, 2018; Branduardi-Raymont  
 325 et al., 2018). If time series of magnetopause images are able to distinguish the local mag-  
 326 netopause deformation, some relevant joint studies can be performed between the global  
 327 magnetopause images and the in-situ magnetopause crossings in the future.

## 328 Open Research Section

329 MMS data are available at the MMS Science Data Center (<https://lasp.colorado.edu/mms/sdc/public/about/browse-wrapper/>), and the solar wind data are acces-  
 330 sible at the CDAweb (<https://cdaweb.gsfc.nasa.gov/pub/data/>). The IRFU-Matlab  
 331 package (<https://github.com/irfu/irfu-matlab>) is used for data analysis. The mag-  
 332 netopause crossing list used in this study can be found at <https://zenodo.org/records/8283060>.  
 333  
 334

## 335 Acknowledgments

336 This work was supported by the National Key R&D Program of China (2021YFA0718600),  
 337 the National Natural Science Foundation of China (grants 42188101, 42122032, 41974196,  
 338 42274211, and 41974170) and the Specialized Research Fund for State Key Laborato-  
 339 ries of China.

## 340 References

- 341 André, M., & Cully, C. M. (2012). Low-energy ions: A previously hidden solar sys-  
 342 tem particle population. *Geophysical Research Letters*, *39*(3).  
 343 Branduardi-Raymont, G., Wang, C., Escoubet, C. P., Adamovic, M., Agnolon, D.,  
 344 Berthomier, M., . . . Zhu, Z. (2018). *SMILE definition study report* (V1.0 ed.;  
 345 Tech. Rep.). ESA/SCI. doi: 10.5270/esa.smile.definition.study\_report-2018-12  
 346 Dmitriev, A., Suvorova, A., & Chao, J.-K. (2011). A predictive model of geosyn-  
 347 chronous magnetopause crossings. *Journal of Geophysical Research: Space*  
 348 *Physics*, *116*(A5). doi: 10.1029/2010JA016208  
 349 Ergun, R., Tucker, S., Westfall, J., Goodrich, K., Malaspina, D., Summers, D., . . .

- 350 others (2016). The axial double probe and fields signal processing for the MMS  
 351 mission. *Space Science Reviews*, 199(1-4), 167–188.
- 352 Escoubet, C. P., Hwang, K.-J., Toledo-Redondo, S., Turc, L., Haaland, S., Aunai,  
 353 N., ... others (2020). Cluster and MMS simultaneous observations of magne-  
 354 tosheath high speed jets and their impact on the magnetopause. *Frontiers in*  
 355 *Astronomy and Space Sciences*, 78.
- 356 Fairfield, D. H. (1971). Average and unusual locations of the Earth's magnetopause  
 357 and bow shock. *Journal of Geophysical Research (1896-1977)*, 76(28), 6700–  
 358 6716. doi: 10.1029/JA076i028p06700
- 359 Hietala, H., Phan, T., Angelopoulos, V., Oieroset, M., Archer, M. O., Karlsson, T.,  
 360 & Plaschke, F. (2018). In situ observations of a magnetosheath high-speed jet  
 361 triggering magnetopause reconnection. *Geophysical Research Letters*, 45(4),  
 362 1732–1740.
- 363 Jacobsen, K., Phan, T., Eastwood, J., Sibeck, D., Moen, J., Angelopoulos, V., ...  
 364 others (2009). Themis observations of extreme magnetopause motion caused  
 365 by a hot flow anomaly. *Journal of Geophysical Research: Space Physics*,  
 366 114(A8).
- 367 Karimabadi, H., Roytershteyn, V., Vu, H., Omelchenko, Y., Scudder, J., Daughton,  
 368 W., ... others (2014). The link between shocks, turbulence, and magnetic  
 369 reconnection in collisionless plasmas. *Physics of Plasmas*, 21(6), 062308.
- 370 Katsavrias, C., Raptis, S., Daglis, I. A., Karlsson, T., Georgiou, M., & Balasis,  
 371 G. (2021). On the generation of Pi2 pulsations due to plasma flow pat-  
 372 terns around magnetosheath jets. *Geophysical Research Letters*, 48(15),  
 373 e2021GL093611.
- 374 LaMoury, A. T., Hietala, H., Plaschke, F., Vuorinen, L., & Eastwood, J. P. (2021).  
 375 Solar wind control of magnetosheath jet formation and propagation to the  
 376 magnetopause. *Journal of Geophysical Research: Space Physics*, 126(9),  
 377 e2021JA029592.
- 378 Li, W. Y., André, M., Khotyaintsev, Y. V., Vaivads, A., Fuselier, S., Graham, D. B.,  
 379 ... others (2017). Cold ionospheric ions in the magnetic reconnection outflow  
 380 region. *Journal of Geophysical Research: Space Physics*, 122(10), 10–194.
- 381 Lin, R. L., Zhang, X. X., Liu, S. Q., Wang, Y. L., & Gong, J. C. (2010). A three-  
 382 dimensional asymmetric magnetopause model. *Journal of Geophysical Re-*  
 383 *search: Space Physics*, 115(A4). doi: 10.1029/2009JA014235
- 384 Lindqvist, P.-A., Olsson, G., Torbert, R., King, B., Granoff, M., Rau, D., ... others  
 385 (2016). The spin-plane double probe electric field instrument for MMS. *Space*  
 386 *Science Reviews*, 199(1-4), 137–165.
- 387 Liu, Z.-Q., Lu, J. Y., Wang, C., Kabin, K., Zhao, J. S., Wang, M., ... Zhao, M. X.  
 388 (2015). A three-dimensional high mach number asymmetric magnetopause  
 389 model from global MHD simulation. *Journal of Geophysical Research: Space*  
 390 *Physics*, 120(7), 5645–5666. doi: 10.1002/2014JA020961
- 391 Ng, J., Chen, L.-J., & Omelchenko, Y. (2021). Bursty magnetic reconnection at the  
 392 earth's magnetopause triggered by high-speed jets. *Physics of Plasmas*, 28(9).
- 393 Nguyen, G., Aunai, N., Michotte de Welle, B., Jeandet, A., Lavraud, B., & Fontaine,  
 394 D. (2022). Massive multi-mission statistical study and analytical modeling of  
 395 the Earth's magnetopause: 2. shape and location. *Journal of Geophysical Re-*  
 396 *search: Space Physics*, 127(1), e2021JA029774. doi: 10.1029/2021JA029774
- 397 Paschmann, G., Haaland, S., Phan, T., Sonnerup, B. Ö., Burch, J., Torbert, R., ...  
 398 others (2018). Large-scale survey of the structure of the dayside magnetopause  
 399 by MMS. *Journal of Geophysical Research: Space Physics*, 123(3), 2018–2033.
- 400 Phan, T. D., & Paschmann, G. (1996). Low-latitude dayside magnetopause and  
 401 boundary layer for high magnetic shear: 1. structure and motion. *Journal of*  
 402 *Geophysical Research: Space Physics*, 101(A4), 7801–7815.
- 403 Plaschke, F., Hietala, H., Angelopoulos, V., & Nakamura, R. (2016). Geoeffective  
 404 jets impacting the magnetopause are very common. *Journal of Geophysical Re-*

- 405 search: *Space Physics*, 121(4), 3240–3253.
- 406 Plaschke, F., Hietala, H., Archer, M., Blanco-Cano, X., Kajdič, P., Karlsson, T., ...  
 407 others (2018). Jets downstream of collisionless shocks. *Space Science Reviews*,  
 408 214, 1–77.
- 409 Plaschke, F., Hietala, H., & Vörös, Z. (2020). Scale sizes of magnetosheath jets.  
 410 *Journal of Geophysical Research: Space Physics*, 125(9), e2020JA027962.
- 411 Pollock, C., Moore, T., Jacques, A., Burch, J., Gliese, U., Saito, Y., ... others  
 412 (2016). Fast plasma investigation for magnetospheric multiscale. *Space Science*  
 413 *Reviews*, 199(1-4), 331–406.
- 414 Russell, C., Anderson, B., Baumjohann, W., Bromund, K., Dearborn, D., Fischer,  
 415 D., ... others (2016). The magnetospheric multiscale magnetometers. *Space*  
 416 *Science Reviews*, 199(1-4), 189–256.
- 417 Šafránková, J., Goncharov, O., Němeček, Z., Přech, L., & Sibeck, D. (2012). Asym-  
 418 metric magnetosphere deformation driven by hot flow anomaly (ies). *Geophysic-*  
 419 *al research letters*, 39(15).
- 420 Schwartz, S. J., Paschmann, G., Sckopke, N., Bauer, T. M., Dunlop, M., Fazaker-  
 421 ley, A. N., & Thomsen, M. F. (2000). Conditions for the formation of hot  
 422 flow anomalies at Earth’s bow shock. *Journal of Geophysical Research: Space*  
 423 *Physics*, 105(A6), 12639–12650.
- 424 Shue, J.-H., Chao, J., Fu, H., Russell, C., Song, P., Khurana, K., & Singer, H.  
 425 (1997). A new functional form to study the solar wind control of the mag-  
 426 netopause size and shape. *Journal of Geophysical Research: Space Physics*,  
 427 102(A5), 9497–9511.
- 428 Shue, J.-H., Chao, J.-K., Song, P., McFadden, J., Suvorova, A., Angelopoulos, V.,  
 429 ... Plaschke, F. (2009). Anomalous magnetosheath flows and distorted sub-  
 430 solar magnetopause for radial interplanetary magnetic fields. *Geophysical*  
 431 *Research Letters*, 36(18).
- 432 Shue, J.-H., Song, P., Russell, C., Steinberg, J., Chao, J., Zastenker, G., ... others  
 433 (1998). Magnetopause location under extreme solar wind conditions. *Journal*  
 434 *of Geophysical Research: Space Physics*, 103(A8), 17691–17700.
- 435 Sibeck, D., Borodkova, N., Schwartz, S., Owen, C., Kessel, R., Kokubun, S., ...  
 436 others (1999). Comprehensive study of the magnetospheric response to a  
 437 hot flow anomaly. *Journal of Geophysical Research: Space Physics*, 104(A3),  
 438 4577–4593.
- 439 Sibeck, D., Kudela, K., Lepping, R., Lin, R., Nemecek, Z., Nozdrachev, M., ... oth-  
 440 ers (2000). Magnetopause motion driven by interplanetary magnetic field  
 441 variations. *Journal of Geophysical Research: Space Physics*, 105(A11), 25155–  
 442 25169.
- 443 Staples, F., Rae, I., Smith, A., Raymer, K., Case, N., Rodger, C., ... others (2020).  
 444 Do statistical models capture the dynamics of the magnetopause during sud-  
 445 den magnetospheric compressions? *Journal of Geophysical Research: Space*  
 446 *Physics*, 125(4), e2019JA027289.
- 447 Toledo-Redondo, S., André, M., Aunai, N., Chappell, C. R., Dargent, J., Fuselier,  
 448 S., ... others (2021). Impacts of ionospheric ions on magnetic reconnec-  
 449 tion and earth’s magnetosphere dynamics. *Reviews of Geophysics*, 59(3),  
 450 e2020RG000707.
- 451 Toledo-Redondo, S., André, M., Vaivads, A., Khotyaintsev, Y. V., Lavraud, B.,  
 452 Graham, D. B., ... Aunai, N. (2016). Cold ion heating at the dayside mag-  
 453 netopause during magnetic reconnection. *Geophysical Research Letters*, 43(1),  
 454 58–66.
- 455 Wang, B., Nishimura, Y., Hietala, H., Lyons, L., Angelopoulos, V., Plaschke, F.,  
 456 ... Weatherwax, A. (2018). Impacts of magnetosheath high-speed jets on  
 457 the magnetosphere and ionosphere measured by optical imaging and satel-  
 458 lite observations. *Journal of Geophysical Research: Space Physics*, 123(6),  
 459 4879–4894.

- 460 Wang, C., & Branduardi-Raymont, G. (2018). Progress of solar wind magnetosphere  
461 ionosphere link explorer(SMILE) mission. *Chinese Journal of Space Science*,  
462 *38*(5), 657–661.
- 463 Wang, X., Lu, J., Wang, M., Zhou, Y., & Hao, Y. (2023). Simultaneous observation  
464 of magnetopause expansion under radial imf and indentation by hsj. *Geophysical*  
465 *Research Letters*, *50*(20), e2023GL105270.
- 466 Xu, Q., Tang, B., Sun, T., Li, W., Zhang, X., Wei, F., ... Wang, C. (2022). Mod-  
467 eling of the subsolar magnetopause motion under interplanetary magnetic field  
468 southward turning. *Space Weather*, *20*(12), e2022SW003250.
- 469 Yang, Z., Jarvinen, R., Guo, X., Sun, T., Koutroumpa, D., Parks, G., ... Wang, C.  
470 (2024). Deformations at Earth's dayside magnetopause during quasi-radial  
471 IMF conditions: Global kinetic simulations and soft X-ray imaging. *Earth and*  
472 *Planetary Physics*, *8*. doi: 10.26464/epp2023059
- 473 Zhang, H., Zong, Q., Connor, H., Delamere, P., Facskó, G., Han, D., ... others  
474 (2022). Dayside transient phenomena and their impact on the magnetosphere  
475 and ionosphere. *Space Science Reviews*, *218*(5), 40.